Anul XXXIX 1994

STUDIA
UNIVERSITATIS BABEŞ-BOLYAI

PHYSICA

2

Editorial Office: 3400 CLUJ-NAPOCA str. M. Kogălniceanu nr.1 ▸ Telefon : 116101

SUMAR - CONTENTS - SOMMAIRE

Spectroscopy

Solid State Physics

Theoretical Physics

STUDIA UNIV. BABEŞ-BOLYAI, PHYSICA, XXXIX, 2, 1994

MAGNETIC FIELD GRADIENT NMR MEASUREMENTS OF THE SELF-DIFFUSION COEFFICIENT OF THE SMALL MOLECULES

M. TODICA*, A. GUILLERMO**, A. V. POP*, G. DAMIAN* and D. CIURCHEA*

ABSTRACT. - Both the constant magnetic field gradient and pulsed field gradient spin-echo NMR methods have been analyzed, to optimise the measurement of the self-diffusion coefficient of the small molecule of simplest liquids or organic solvents. We propose a method in order to eliminate the effect of the residual magnetic field gradient in the computing the self-diffusion coefficient of small molecules of pure liquids. We have used this method to calculate the self-diffusion coefficient of the pure cyclohexane in the 260 K to 335 K temperature range.

INTRODUCTION

The study of the diffusion of small molecules is of great interest to characterise the dynamics and structure of the pure liquids, organic solvents or polymeric solutions. It is possible to measure directly the self diffusion coefficient using radioactive tracer, but also using the magnetic field gradient spin-echo NMR technique. The NMR technique presents certain advantages giving the possibility to evaluate the self-diffusion coefficients over a large range, from fast diffusion (above 10^{-6} cm^2/s) to very slow diffusion (10^{-14} cm^2/s) [1]. The diffusing molecules are not perturbed by the method and moreover, the technique can provide individual self-diffusion coefficients from mixtures of diffusing molecules without the need of the isotopic labelling.

* *"Babeş-Bolyai" University, Faculty of Physics, 3400 Cluj-Napoca, Romania*
** *Lab. Spectrometrie Physique, CERMO, Grenoble, France.*

MEASUREMENTS OF THE SELF-DIFFUSION COEFFICIENT

The measurement of the self-diffusion coefficient by the NMR techniques is based on the additional attenuation of the spin-echo obtained with a classical RF pulse sequence $\pi/2-\tau-\pi-\tau-echo$, when a magnetic-field gradient is superimposed over the main magnetic field $\vec{B}_0$ [2].

If the amplitude of the magnetic field gradient is constant in time, the amplitude of the spin-echo A(2τ) reported to the initial amplitude A(0) is described by the equation:

$$\ln \frac{A(2\tau)}{A(0)} = -\frac{2\tau}{T_2} - \frac{1}{12} D\gamma^2(2\tau)^3\vec{G}_t^2 \qquad (1)$$

where D is the self-diffusion coefficient, γ the gyromagnetic factor and $\vec{G}_t=\vec{G}+\vec{G}_r$ the total magnetic gradient including the residual magnetic gradient $\vec{G}_r$. This gradient is due to the inhomogenities of the magnetic field over the sample volume and generally it is much smaller than the applied gradient $\vec{G}$.

This method is used to measure self-diffusion coefficients greater than 10^{-7} cm^2/s. Much smaller self-diffusion coefficient, D ≤ 10^{-14} cm^2/s can be measured using the pulsed-field magnetic gradient NMR method as first described by Stejskal and Tanner [3]. The magnetic field gradient is applied in the form of two pulses of magnitude G, duration δ and separation Δ (fig.1).

The NMR sequence is $\pi/2-G(\delta)-\pi-G(\delta)-echo$.

The amplitude of the spin - echo is given by the equation:

$$\ln \frac{A(2\tau)}{A(0)} = -\frac{2\tau}{T_2} - \gamma^2 D[\frac{2}{3}\tau^3 G_r^2 + \delta^2(\Delta - \frac{\delta}{3})G^2 - K\vec{G}\vec{G}_r] \qquad (2)$$

T_2 is the spin-spin time relaxation and K is a function determined by the gradient pulse-sequence.

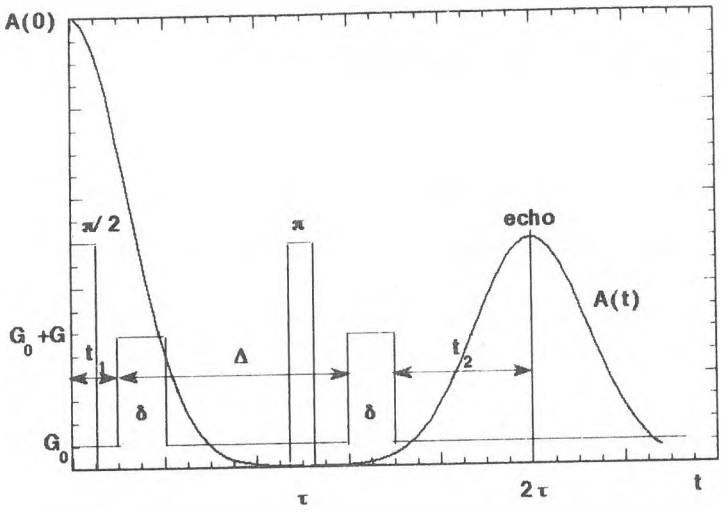

Fig. 1. The pulsed-field magnetic NMR sequence.

$$K=\delta[t_1^2+t_2^2+\delta(t_1+t_2)+\frac{2}{3}\delta^2-2\tau^2] \tag{3}$$

The time intervals t_1 and t_2 are defined on the figure 1.

In both the cases the self-diffusion coefficient is usually determined by varying the time intervals of the NMR pulse -sequence or the amplitude of the magnetic gradient [4, 5, 6].

The effect of the residual gradient $\vec{G}_r$ is generally neglected. Results are in good agreement with those obtained using other methods.

In this paper, we propose a method to eliminate the effect of the residual gradient for calculation self-diffusion coefficient, based on the classical spin-echo pulse sequence $\pi/2-\tau-\pi-\tau-echo$. The magnetic gradient is pulsed or time constant, as was previously described. All the time intervals were kept constants and only the amplitude of the magnetic field gradient is varied. The amplitude $A(2\tau)_G$ of the spin-echo is divided by the amplitude

$A(2\tau)_{G=0}$ of the spin-echo which correspond at G = 0 in order to eliminate the relaxation time T_2. In the case of the constant gradient equation (1) became:

$$\ln \frac{A(2\tau)_G}{A(2\tau)_{G=0}} = -\frac{2\gamma^2 D\tau^3}{3}[G^2+2GG_0] \quad (4)$$

where G_0 is the projection of $\vec{G}_r$ on the direction of $\vec{G}$. When G_r is much small than G the equation (4) can be considered linearly on G^2. The self-diffusion coefficient D can be calculate from the slope of the straight line corresponding to this representation, but this value will be affected by G_0.

We can separate the contribution of the external gradient G from those of the residual G_0 gradient if we use the relations:

$$\frac{1}{G}\ln \frac{A(2\tau)_G}{A(2\tau)_{G=0}} = -\frac{2\gamma^2 D\tau^3}{3}[G + 2G_0] \quad (5)$$

In the case of the pulsed field gradient method, equation (2) became:

$$\frac{1}{G}\ln \frac{A(2\tau)_G}{A(2\tau)_{G=0}} = -\gamma^2 D[\delta^2(\Delta-\frac{1}{3}\delta)G-KG_0] \quad (6)$$

Equations (5) and (6) are linearly in G and the self-diffusion coefficient is calculated directly from the slopes of the straight lines corresponding of those representations. The residual gradient G_0 was determined from the ordinate at the origin of this straight line. In this case the value of the D is not affected by the residual gradient G_0.

RESULTS AND DISCUSSIONS

All measurements have been performed using a Bruker CXP spectrometer with a measuring frequency of 36 MHz. A home-built apparatus made on the basis of the reference [7] was used to obtain the magnetic gradient pulses. A pair of anti Helmholtz coils provided the linear gradient field. The gradient intensity is determined by the current intensity I in the

coils and by a constant α depending on the coil geometry: $G = \alpha I$, [8,9]

The gradient field was calibrated by using distilled water as a test sample and by measuring the attenuation of the spin-echo amplitude when the apparatus work in steady gradient. α and G_0 were calculated by fitting the linear representation $\frac{1}{I} \ln \frac{A(2\tau)_G}{A(2\tau)_{G=0}}$ versus I (I>0),

$$\frac{1}{I} \ln \frac{A(2\tau)_G}{A(2\tau)_{G=0}} = -\frac{2\gamma^2 D\tau^3}{3}[\alpha^2 I + 2\alpha G_0] \qquad (7)$$

derived from equation (5). The constant α was determined from the slope of this straight line and the known value of the self-diffusion coefficient of this samples: $D = 2.266\ 10^{-5}$ cm^2/s at 298 K [10], (fig. 2). Two diffusion times have been utilised τ = 12.5 ms and τ = 17.5 ms. In both the cases we found α =14.01 ± 0.06 gauss/cm /A and G_0 = 0.20 ± 0.05 gauss/cm and the residual gradient G_0 was determined by the ordinate at the origin of the straight line.

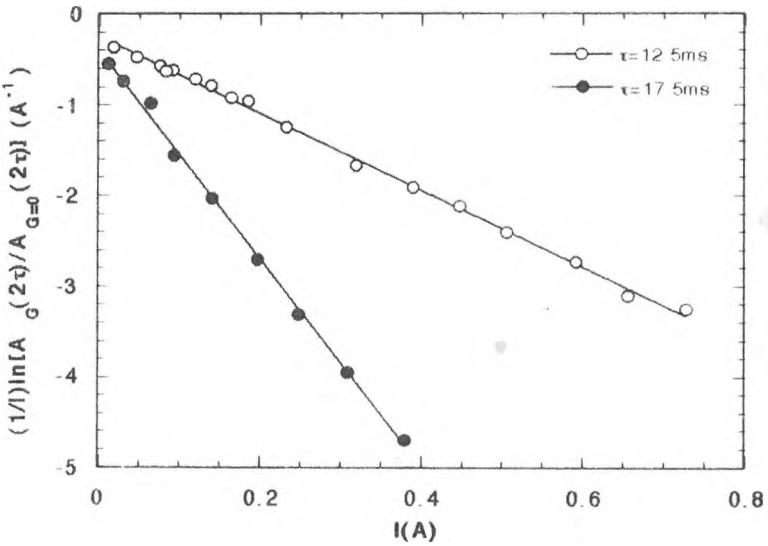

Fig. 2 Spin-echo attenuation of the test samples when a constant magnetic gradient field was applied.

To verify the validity of the calibration and the advantages of the use of equation (5) and (6) to calculate the self-diffusion coefficient, we used the pulsed field gradient method to measure the self-diffusion coefficient of the water. We used the NMR pulse-sequence described previously with constant time intervals, and the value of α calculated from the constant field gradient method (α = 14.01 gauss/cm/A). The gradient was varied within the range 0 - 80 gauss/cm. We performed two series of experiments for evaluation the spin-echo attenuation for δ = 2.5ms and δ = 6ms. The self-diffusion coefficient of the water was calculated by the slope of the linear representation $\frac{1}{G}\ln\frac{A(2\tau)_G}{A(2\tau)_{G=0}}$ versus G, (G>0) described by equation. (6) (fig.3). In both the cases we found the value D = 2.26 10^{-5} cm^2/s $\pm$ 0.02 cm^2/s.

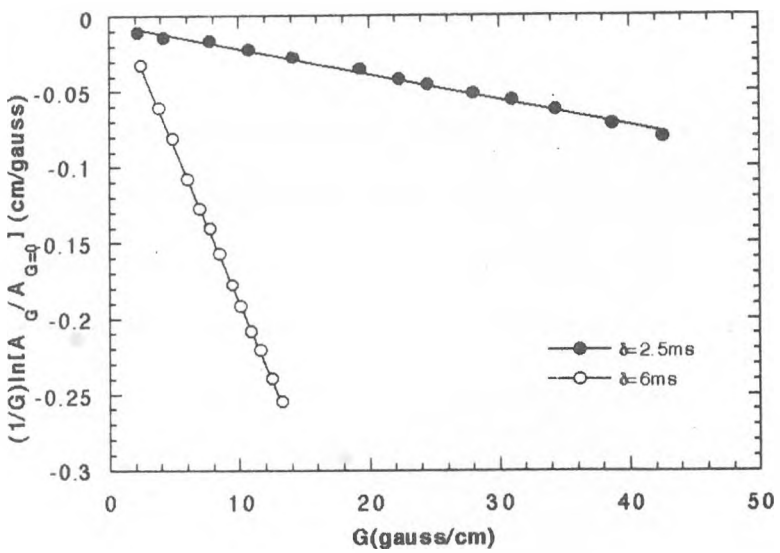

Fig. 3. Spin-echo attenuation of water when a pulsed-magnetic gradient field was applied.

This method presents certain advantages: the diffusion time is constant during all the measurement, the contribution of the residual gradient is eliminated and the gradient can be

varied in a large range.

Another method to eliminated the effect of the residual gradient is based on the variation of the length δ of the gradient pulses at constant field gradient. The time intervals t_1 and Δ were kept constant and only the pulse length δ and the interval time t_2 were varied , respecting the condition $\delta+t_2=t_1+\Delta=const$. For each value of the pulse length we measured the amplitudes of the spin-echo $A(2\tau)_{G1}$ and $A(2\tau)_{G2}$ for two constant values of the magnetic field gradient G_1 and G_2.

From the equation (2) we obtained:

$$\ln \frac{A(2\tau)_{G_1}}{A(2\tau)_{G_2}} = -\gamma^2 D[\delta^2(\Delta-\frac{1}{3}\delta)(G_1^2-G_2^2)-K(G_1-G_2)G_0] \qquad (8)$$

This equation leads to a linear representation of the attenuation of the spin-echo versus the $\delta^2(\Delta-\delta/3)$ variable. Experimental data for water, at T=298K, are presented in the Fig. 4.

The self-diffusion coefficient is calculated from the slope of the straight line and the value of α = 0.140 gauss/cm/A obtained in the constant gradient method. The value $D=2.236.10^{-5}$ cm^2 /s ± 0.04 cm^2 /s is in good agreement with the previous results.

This method may also eliminate the effect of the residual gradient in the computing of the self-diffusion coefficient and results obtained for D are in good agreement with those of other methods. However there are the inconvenient that the length of the gradient pulses do not overcome the time delay τ within the RF pulses.

Results obtained in our tests confirm that the representation described by equation (6) can be use to calculate the self-diffusion coefficient with a great accuracy.

Finally we used this representation to calculate the self-diffusion coefficient of the pure cyclohexane in the temperature range of 280 at 334 K.

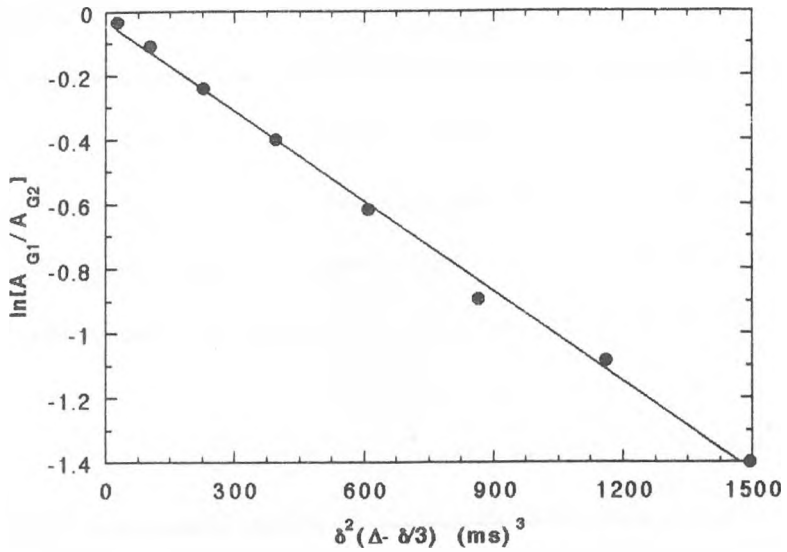

Fig. 4.Spin-echo attenuation of the water when a pulsed magnetic gradient-field of variable length was applied.

The temperature dependence of D is presented in the figure 5.

Results obtained are in good agreement with the literature [10].

CONCLUSIONS

The constant magnetic gradient field NMR technique and the pulsed-magnetic gradient field NMR technique can be used to measure the self-diffusion coefficient of the small molecules of the pure liquids. The contribution of the residual magnetic gradient field is eliminated by the use of the representations described by the equations (5) and (6). This method is validate by the results obtained in the measurement of the self-diffusion coefficient of test samples of water. The self-diffusion coefficient of pure cyclohexane was measured using this method. Results obtained were in good agreement with the literature.

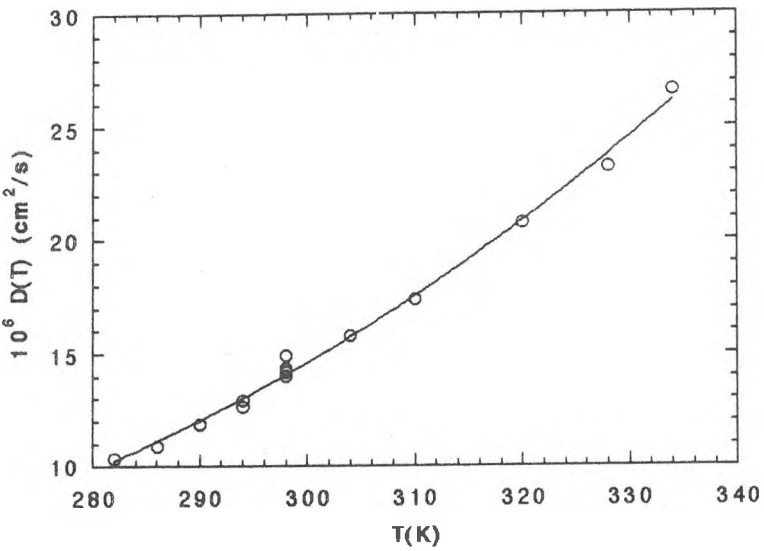

Fig.5. Temperature dependence of the self-diffusion of pure cyclohexane.

REFERENCES

1. Stilbs P., Progr. Nucl. Magn. Reson. Spectrosc. 1987, 19, 1.
2. Carr H. Y. and Purcell E. M., Phys. Rev. 1954, 94, 631.
3. Stejskal E. O., Tanner J. E., J. Chem. Phys. 1965, 42, 288.
4. Zhu X. X., and Macdonald P. M., Macromol. 1992, 25, 4345.
5. Davis P. J., Pinder D. N., and Callaghan P. T., Macromol. 1992, 25, 170.
6. Fleischer G., Fujara F., Macromol. 1992, 25, 4210.
7. Callaghan P. T., Trotter C. M., Jolley K. W., J. Mag. Res. 1980, 37, 247.
8. Ursu I., Demco E.D., Bălibanu F., Bogdan M., Gligor D., Dollinger R., Pop G., Groza D., Gorgan D., Bogdan A.M., Nedevski S., Rev. Roum. Phys., 1989, 34, 59.
9. Nicula Al., Aştilean S., Todică M. and Nicula S., Studia UBB, Physica, XXXII, 2, 1987, 35.
10. Marc C. Piton, Robert G. Gilbert, Bogdan E. Chapman and Phillip W. Kuchel, Macromol. 1993, 26, 4472.

STUDIA UNIV. BABEŞ-BOLYAI, PHYSICA, XXXIX, 2, 1994

RAMAN SPECTROSCOPIC INVESTIGATIONS OF THE STRUCTURE OF $3B_2O_3áK_2O$ GLASSES WITH TRANSITION METAL IONS

D. MANIU*, I. ARDELEAN* and T. ILIESCU*

ABSTRACT. - The influence of the transition metal (TM) oxides (V_2O_5, CuO, NiO, Fe_2O_3, TiO_2, CoO, Cr_2O_3, MnO) on the structure of $3B_2O_3áK_2O$ glass was investigated by Raman spectroscopy. Adding TM oxides a change of a relative proportion of different structural groups was observed. The appearance of new structural groups (i.e. ring type metaborate groups for Fe_2O_3, CuO and NiO and diborate groups for Fe_2O_3, NiO and Cr_2O_3) was also observed. The addition of Cr_2O_3 determines also the incorporation of a second BO_4 tetrahedron into a pentaborate group in resulting the formation of a dipentaborate group. Therefore TM ions acts as modifier of the network in the studied glasses.

1. INTRODUCTION

Raman spectroscopy has proved to be a useful tool in the study of vitreous oxide materials. Raman spectra of crystalline borates have been used as a basis for the qualitative identification of glass forming structural units in borate glasses [1-3]. The introduction of the transition metal (TM) oxides in the glasses lead to the change of the glass structure, TM ions acting as modifier [4-6].

In this study we have investigated by Raman spectroscopy in the (200-1600 cm^{-1}) spectral range the structural units present in $xMOá(1-x)[3B_2O_3áK_2O]$ glasses at two molar concentrations for the TM oxides MO (MO = V_2O_5, CuO, NiO, Fe_2O_3, TiO_2, CoO, Cr_2O_3, MnO).

* *"Babeş-Bolyai" University, Faculty of Physics, 3400 Cluj-Napoca, Romania*

2. EXPERIMENTAL

In order to obtain further information of the TM ions influence on the structure of alkali borate glasses, we investigated the xMOá(1-x)[$3B_2O_3$áK_2O] glasses with x = 0.005; 0.01 and MO = V_2O_5, CuO, NiO, Fe_2O_3, TiO_2, CoO, Cr_2O_3, MnO maintaining the B_2O_3/K_2O ratio constant. These glasses were prepared by mixing H_3BO_3, K_2CO_3 and MO in suitable proportions and melting this mixture in sintered corundum crucibles at T = 1200°C for 0.5 h. The parallelepiped shaped samples were obtained by pouring of melts in stainless steel forms.

The Raman spectra have been recorded on a GDM 1000 double monochromator instrument equipped with ILA 120-1 argon-ion laser; the emission line at 488 nm was used with a incident power of about 0.80 W. A 90° geometry and a spectral slit width of 3-4 cm^{-1} was used for collecting the scattered light. The spectra was recorded without polarizer in the gathering optics. The measurements were carried out at room temperature.

3. RESULTS AND DISCUSSION

It is well known that the Raman spectrum of pure B_2O_3 has one very strong band at about 806 cm^{-1}. This frequency characterizes the specific ring structure of the B_2O_3 glass. Furukawa and White [7] and Galmer [8] have assigned this band to the symmetric breathing motion of boroxol rings. The addition of K_2O to the borate glass promotes the breakdown of boroxol rings and helps in the formation of BO_4 tetrahedral units. The experimental evidence for such a process is the appearance of a Raman band at 770 cm^{-1} together with a decrease in the intensity of the band at 806 cm^{-1}. The Raman band centered at 770 cm^{-1} which appears

in this case is assigned by Bril [3] to the formation of six membered rings containing one BO_4 tetrahedron (i.e. triborate, tetraborate or pentaborate) and the shift of this band towards lower frequency (~ 755 cm^{-1}) has been assigned to six membered rings with two BO_4 tetrahedra (i.e. ditriborate or dipentaborate).

Crystalline Na_2O-$2B_2O_3$ which is made up of ditriborate groups and dipentaborate groups has a dominant band at 755 cm^{-1} [1]. Raman spectra of crystalline α- and β- K_2O-$5B_2O_3$ which consist of pentaborate groups have been recorded by Konijnendijk [1]. The α form has bands at 765, 885 and 650 cm-1 with a number of close lying bands in the region of 500 cm^{-1}. The β form presents vibrational bands at 785, 925 and 625 cm^{-1} with a few more close lying bands around 500 cm^{-1}. Hence pentaborate groups could be identified by the simultaneous presence of the 770, 930 and 650 cm^{-1} bands along with considerable scattering in the 500 cm^{-1} region [6]. Triborate and tetraborate groups give rise to the 770 cm^{-1} band and a weak band at 930 cm^{-1} but no bands in the 660 cm^{-1} spectral region [1]. Hence the 770 cm^{-1} band can not be taken alone to indicate the presence of a particular group. The diborate groups are identified by the presence of a band around 1050 cm^{-1} [2]. Raman spectra of ZnO-$2B_2O_3$ and Li_2O-$2B_2O_3$ which consist of diborate groups show vibrational bands around 1050 and 980 cm^{-1} and at 1035, 980 and 930 cm^{-1}, respectively [1, 9]. Therefore the band at 1050 cm^{-1} is assigned to diborate groups.

By comparison with the spectra of crystalline CaO-B_2O_3 and Li_2O-B_2O_3 which are known to contain chain-type metaborate group, the 660-670 cm^{-1} and 1450-1500 cm^{-1} bands are assigned to the chain metaborate groups [2]. Konijnendijk [1] showed that a number of crystalline borate compounds containing six membered rings with BO_4 tetrahedra (such as

pentaborate, triborate, diborate, etc.) give Raman bands in the 450-500 cm^{-1} region. Kamitsos et al. [2] presume that is nearly impossible to assign the observed bands to a specific structural group. The band centered at 460 cm^{-1} is assigned to a ring angle bending (B-O-B) from BO_4 tetrahedra [10] which was observed at 470 cm^{-1} for pure B_2O_3 [11].

The band centered at 600-620 cm^{-1} is known to originate from vibrations of the ring type metaborate groups. Bril [1] assigned this band to the metaborate ring breaking vibration which involves the displacement of all oxygen atoms, based on the Raman spectrum of the Cs_2O-B_2O_3 which contain ring type metaborate groups.

By comparison with Raman spectra of crystalline pyroborate $2Li_2O$-B_2O_3 the band centered at 1210 cm^{-1} is assigned to pyroborate groups [10].

The strongest band in the Raman spectra of the Mg- and Ca-orthoborate compounds is observed at 920 and 930 cm^{-1}, respectively. Thus the band centered at ~ 930 cm^{-1} was assigned to orthoborate group [9, 10].

Our Raman spectra of potassium borate glasses of the xMOá(1-x)[$3B_2O_3$áK_2O] system with MO = V_2O_5, CuO, NiO, Fe_2O_3, TiO_2, CoO, Cr_2O_3, MnO atand x = 0 and 0.005 are shown in Figs 1 and 2.

As is shown the bands centered at ~ 450 cm^{-1}, ~ 600 cm^{-1}, ~ 670 cm^{-1}, ~ 770 cm^{-1}, ~ 800 cm^{-1}, ~ 920 cm^{-1}, ~ 1045 cm^{-1}, ~ 1250 cm^{-1} and ~ 1460 cm-1 are presented. The band centered at 806 cm^{-1} is shifted at low frequency, ~ 800 cm^{-1}.

For the studied glasses, the intensity of 770 cm^{-1} band is greater than that of 800 cm^{-1}, therefore the number of borate rings is higher that the number of boroxol rings (Fig.3a).

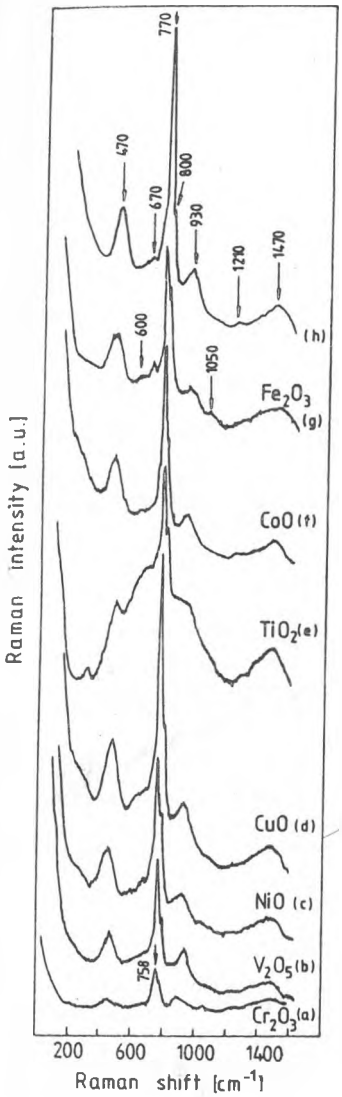

Fig. 1. Raman spectra of the $xMnOá(1-x)[3B_2O_3áK_2O]$ glass system with x = 0.005 and
(MO = Cr_2O_3 (a), V_2O_5 (b), NiO (c), CuO (d), TiO_2 (e), CoO (f), Fe_2O_3 (g), x = 0 (h).

A detailed inspection of the Raman spectra shows that the 770 cm^{-1} band is present along with the bands at 930 cm^{-1}, 670 cm^{-1} and considerable scattering in the 500 cm^{-1} region. It appears that in the studied glasses, the boroxol rings are converted to pentaborate groups and not to tetraborate or triborate groups.

Raman spectrum of $3B_2O_3áK_2O$ (Fig. 1 h) is dominated by the band due to the symmetric breathing vibration of six membered rings with one BO_4 tetrahedron (770 cm^{-1}). This band reflects the existence of a pentaborate groups (Fig. 3 b). In $3B_2O_3áK_2O$ glass orthoborate (930 cm^{-1}) (Fig. 3 c), chain type metaborate (670 cm^{-1} and 1470 cm^{-1}) (Fig. 3 d) and pyroborate (1210 cm^{-1}) (Fig. 3 e) groups also appear.

In Raman spectra of $xV_2O_5á(1-x)[3B_2O_3áK_2O]$ (Fig. 1 b); $xCoOá(1-x)[3B_2O_3áK_2O]$ (Fig. 1 f) and $xTiO_2á(1-x)[3B_2O_3áK_2O]$ (Fig. 1 e) with x = 0.005 the following bands are present: 770 cm^{-1} (pentaborate groups), 800 cm^{-1} (boroxol rings), 470 cm^{-1} (B-O-B from BO_4 tetrahedra), 930 cm^{-1} (orthoborate groups), 670 cm^{-1} and 1480 cm^{-1} (chain type metaborate groups) and 1210 cm^{-1} (pyroborate groups) and a band centered at ~ 300 $cm^{-1}$for TiO_2.We observed that the

addition of these TM oxides do not determine the appearance of a new structural groups, but only a change of the proportion of these groups which is reflected in the change of the relative intensity of the corresponding bands (Table 1). The addition of TiO_2 determines an important change of the structural groups and of the relative intensities respectively: the band at 670 cm^{-1} became higher than those at 470 and 930 cm^{-1}. Therefore with addition of TiO_2 the number of the chain type metaborate groups became higher than the number of the orthoborate groups.

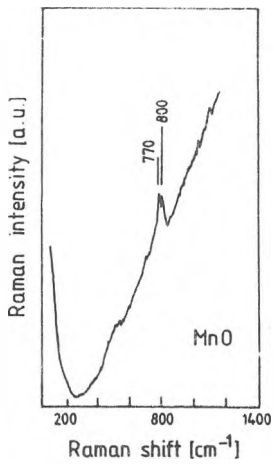

Fig. 2. Raman spectrum of the xMOá(1-x)[$3B_2O_3$áK_2O] glass with x = 0.005.

Table 1. Structural groups present in the xMOá(1-x)[$3B_2O_3$áK_2O] glass system (x = 0.005; MO = V_2O_5, TiO_2, CoO, CuO, NiO, Fe_2O_3, Cr_2O_3) and the relative intensities of the corresponding bands, rationed to the intensity of the 770 cm^{-1} band (758 cm^{-1} band for Cr_2O_3).

	$3B_2O_3$· K_2O	V_2O_5	TiO_2	CoO	CuO	NiO	Fe_2O_3	Cr_2O_3
Boroxol (~800cm^{-1})	0.43	0.58	0.72	0.24	0.45	0.69	0.78	0.65
Pentaborate (~770cm^{-1})	1	1	1	1	1	1	1	-
Dipentaborate (~758cm^{-1})	-	-	-	0.22	-	-	-	1
Orthoborate (~930cm^{-1})	0.2	0.35	0.37	0.03	0.2	0.24	0.25	-
Pyroborate (1210cm^{-1})	0.03	0.06	0.07	0.27	0.02	0.04	0.06	0.07
Chain type metaborate (~670cm^{-1})	0.24	0.34	0.55	-	0.25	0.33	0.38	0.17
Ring type metaborate (~600cm^{-1})	-	-	-	-	0.23	0.27	0.29	-
Diborate (~1050cm^{-1})	-	-	-		-	0.1	0.1	0.1

In Raman spectrum of xCuOá(1-x)[$3B_2O_3$áK_2O] (Fig. 1 d) with x = 0.005 the following bands are present: 770 cm^{-1} (pentaborate groups), 800 cm^{-1} (boroxol rings), 470 cm^{-1} (B-O-B from BO_4), 670 and 1460 cm^{-1} (chain type metaborate groups), 925 cm^{-1}

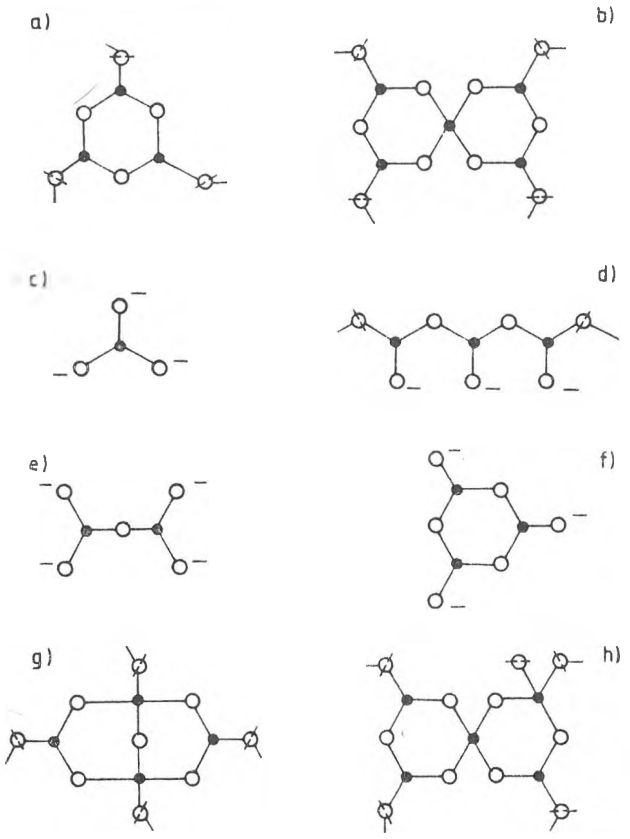

Fig 3. Typical structural groups present in the borate glass: a)boroxol group; b)pentaborate group, c)orthoborate group, d)chain type metaborate group, e)pyroborate group, f)ring type metaborate group, g)diborate group, h)dipentaborate group. Solid circles represent boron atoms, open circles, oxygen atoms. Note that Ø indicates a bridging and O non bridging oxygen.

(orthoborate groups) 1220 cm^{-1} (pyroborate groups) and 600 cm^{-1} (ring type metaborate groups) (Fig. 3 f). From these data results that the addition of the TM oxide determine the appearance of the ring type metaborate groups and a change of the relative intensities of the Raman bands (Table 1).

In Raman spectra of $xFe_2O_3á(1-x)[3B_2O_3áK_2O]$ and $xNiOá(1-x)[3B_2O_3áK_2O]$ (Fig.

1 e and c) with x = 0.005 the following bands are present : 770 cm^{-1} (pentaborate groups); 800 cm^{-1} (boroxol rings); 470 cm^{-1} (B-O-B from BO_4), 670 and 1470 cm^{-1} (chain type metaborate groups), 925 cm^{-1} (orthoborate groups), 1050 cm^{-1} (diborate groups) (Fig. 3 g), 1220 cm^{-1} (pyroborate groups) and 600 cm^{-1} (ring type metaborate groups). From these data results that the addition of Fe_2O_3 and NiO determines the forming of the ring type metaborate and of the diborate groups and the change of the relative intensities of the Raman bands.

In Raman spectrum of $xCr_2O_3á(1-x)[3B_2O_3áK_2O]$ with x = 0.005 (Fig. 1 a) the following bands are present: 758 cm^{-1} (dipentaborate groups) (Fig. 3 h), 800 cm^{-1} (boroxol rings), 450 cm^{-1} (B-O-B from BO_4), 660 and 1470 cm^{-1} (chain type metaborate groups), 900 cm^{-1} and 1050 cm^{-1} (diborate groups) and 1210 cm^{-1} (pyroborate groups). From these data results that the addition of Cr_2O_3 determines the forming of the diborate groups and the incorporation of a second BO_4 tetrahedron into a pentaborate group and as a result, the formation of a dipentaborate group.

Raman spectrum of $xMnOá(1-x)[3B_2O_3áK_2O]$ system with x = 0.005 (Fig. 2) are dominated by the fluorescence, but we can see the bands from 770 cm^{-1} and 800 cm^{-1}. The presence of the fluorescence which covers the Raman bands, do not allow to establish what kinds of structural groups are present in this glass.

We also recorded the Raman spectra of $xMOá(1-x)[3B_2O_3áK_2O]$ with x = 0.01 and MO = V_2O_5, NiO, CuO, Fe_2O_3, TiO_2, MnO, but this spectra do not present a significant changes from those with x = 0.005.

4. CONCLUSIONS

The adding of TM oxides in $3B_2O_3áK_2O$ glass determines a modification of a relative proportion of a different structural groups and the appearance of a new structural groups.

The adding of Fe_2O_3, CuO and NiO determines the forming of ring type metaborate groups, whereas the introduction of Fe_2O_3, NiO and Cr_2O_3 determines the forming of diborate groups. The adding of Cr_2O_3 determines the transformation of the pentaborate groups in the dipentaborate groups. The adding of TiO_2 determines the strongest modification in the intensity of the Raman bands and involves the changes of the ratio between different structural groups.

From these data results that the all studied TM ions act as modifiers of the network in the glass under investigation.

REFERENCES

1. W.L.Konijnendijk, Philips Res. Rep. Suppl. 1, 243 (1975)
2. E.J.Kamitsos, M.A.Karakassides & G.D.Chryssikos, Phys. Chem. Glasses 30, 229 (1989)
3. T.W.Bril, Philips Res. Rep. Suppl. 2, 117 (1976)
4. T.Iliescu, S.Simon, D.Calugar, J. Molec. Struct. 267, 231 (1992)
5. T.Iliescu, S.Simon, D.Maniu, I.Ardelean, J. Molec. Struct. 294, 201 (1993)
6. B.N.Meera, J.Ramakrishna, J. of Non-Cryst. Solids, 159, 1 (1993)
7. F.L.Galneer, Solid State Commun. 44, 1037 (1982)
8. T.Furukawa, W.B.White, Phys. Chem. Glasses 21, 85 (1982)
9. B.N.Meera, A.K.Sood, N.Chanbdrabhas, J.Ramakrishna, J. of Non-Cryst. Solids, 126, 224 (1990)
10. W.L.Konijnendijk, J.M.Stevels, Borate Glasses, Mat. Sci. Res. 12 (1977) 259 (Plenum New York)
11. J.Krogh-Moe, Phys. Chem. Glasses 6, 46 (1965).

STUDIA UNIV. BABEŞ-BOLYAI, PHYSICA, XXXIX, 2, 1994

PENTACENE DOPED BENZOIC ACID CRYSTAL - A MODFL FOR NONPHOTOCHEMICAL HOLE BURNING OF IMPURITY ELECTRONIC TRANSITION IN ORGANIC GLASSES

S. AŞTILEAN*, T. ILIESCU*, Z. TANKO*, S. CÎNTA*, D. MANIU* and I. BRATU**

ABSTRACT. - Optical excitation at liquid helium temperature of pentacene molecules embedded in benzoic acid crystals gives rise to defects in the environment of pentacene. It has been proven that these defects are produced by reversible proton transfer between the benzoic acid host and the pentacene guest. The defect sites are unstable and decay with lifetimes ranging from second to hours. Different defect sites also interconvert spontaneously in the dark or after absorption of a second photon. This ensemble of pentacene molecules in defect environment exhibits many of characteristics which are commonly observed for dye molecules dissolved in glasses (i.e. hole burning, spectral diffusion, etc.) and, therefore, represents in many regards a model of these more complex amorphous systems.

1. INTRODUCTION

The burning of persistent holes (dips) in the site inhomogeneously broadened absorption bands of organic molecules imbedded in low temperatures matrices has become an important topic over the past decade. Beyond its potential use for optical memories this phenomenon has proven to be the most useful line narrowing technique in optical spectroscopy of condensed phases [1-3]. The hole production resulted from irradiation with a narrow line laser in a impurity vibronic absorption band associated with the lowest singlet (S_1) absorption system. By the term *persistent* it is generally meant that the spectral holes (dips) last for time periods longer that the lifetime of any excited state with no profile change, provided the samples is maintained at below the temperature at which the holes are burned and in the dark. Obviously, this type of solid state hole burning has its origin in mechanisms

* *"Babeş-Bolyai" University, Faculty f Physics, 3400 Cluj-Napoca, Romania*

** *Institute of Isotopic and Molecula Technology, P.O. Box 700, 3400 Cluj-Napoca, Romania*

very different from that operative in transient saturation hole burning spectroscopy [4].

Persistent spectral hole burning often occurs in disordered solids as glasses or polymers, where the glassy material is used as host material for color center-like states of dye molecule. The mechanisms of spectral changes observed after optical excitation of absorbing guest can be divided into two classes:

1) photochemical hole burning (PHB) where the spectral changes are produced through the photochemistry of the absorbing specie in the matrix, and

2) non-photochemical hole-burning (NPHB) where the absorbing specie is not altered after the excitation-relaxation cycle and the spectral changes are produced through photoinduced microscopic rearrangements of the matrix itself.

The mechanisms leading to the bleaching of the absorption of dye molecule are important for the understanding of the nature of these materials (host-guest interactions, local photochemistry) and, consequently, for its molecular applications (optical data storage systems). While several mechanisms have been identified (dissociation, ionization and electron transfer, proton transfer), others photoinduced changes are more subtle and involve rearrangements of dye-host system which are not so well characterized and understood. In organic glasses, in particular, it has been suggested that two-level tunneling systems are involved in the formation of holes but the precise nature of these has not been elucidated yet. Holeburning could always be observed in hydrogen bonded solids and the hole formation and evolution was shown to depend strongly on deuteration, suggesting rearrangements of the hydrogen bond networks [5]. The complexity of the inhomogeneous distribution of local environments, reaction and relaxation rates makes precise observations more difficult in

amorphous hosts.

Crystalline host materials are better adapted for such studies and can be used as *model* for situations encountered also in glasses.

Recently, one of authors (S.A.), have studied the photoinduced proton transfer in the mixed molecular crystals, namely pentacene doped a hydrogen bonded crystals of benzoic acid [6].

The present paper discuss some ideas about the possibility to take the phototransformation observed in pentacene doped benzoic acid (PC/BA), a *crystalline material*, as a model for a NPHB process observed in glasses. This idea comes from the fact that the irradiated PC/BA crystals exhibits many properties, i.e. hole burning, spectral diffusion, etc., which are also commonly observed for dye molecules dissolved in glasses. Our analysis show that the ensemble of pentacene molecules in defect environments can be regarded as a disordered solid and that this ensemble of metastable defects sites represents in many regards a *model* of more complex amorphous system.

2. PENTACENE IN BENZOIC ACID CRYSTAL

A. Spectroscopic survey. The pentacene molecule and benzoic acid dimer have similar sizes and have both a center of symmetry. In the benzoic acid host crystal, pentacene occupies a single substitutional site where pentacene replaces one benzoic acid dimer (Fig. 1).

The absorption spectrum at liquid helium temperatures (1.8 K) of PC in BA cystal is typical of mixed molecular crystal showing one sharp (fwhm<1 cm^{-1}) electronic origin line at 16 998.3 cm^{-1}, accompanied by phonon side band and vibronic origins (Fig. 2 (a)). Optical

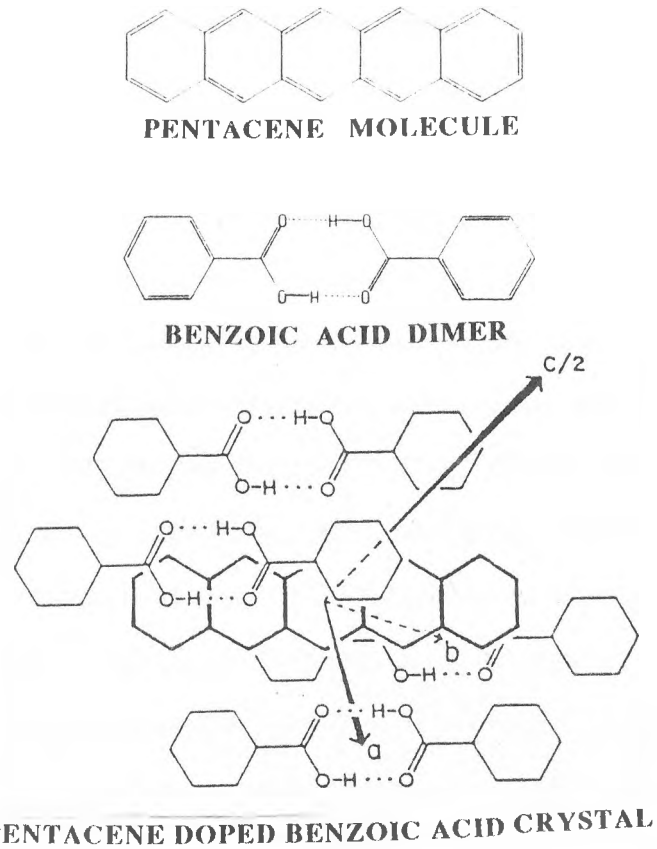

Fig. 1: Pentacene and benzoic acid dimer drawn on the same scale (top). Structure of pentacene doped benzoic acid crystal (bottom).

irradiation in the pentacene spectrum leads to bleaching of the absorption ant to appearance of a large number of new absorption lines (Fig. 2 (b)). The spectral dips or *hole burning* in the absorption spectrum is observed when a laser selective irradiation was applied.

All the photoinduced spectral changes disappear spontaneously in the dark and the original absorption spectrum is restored in the lifetimes ranging from subsecond to tens hours. Since the vibronic progression observed for these new "photosites" is identical to the progression of the stable site, these absorption lines have been assigned to *unaltered* PC

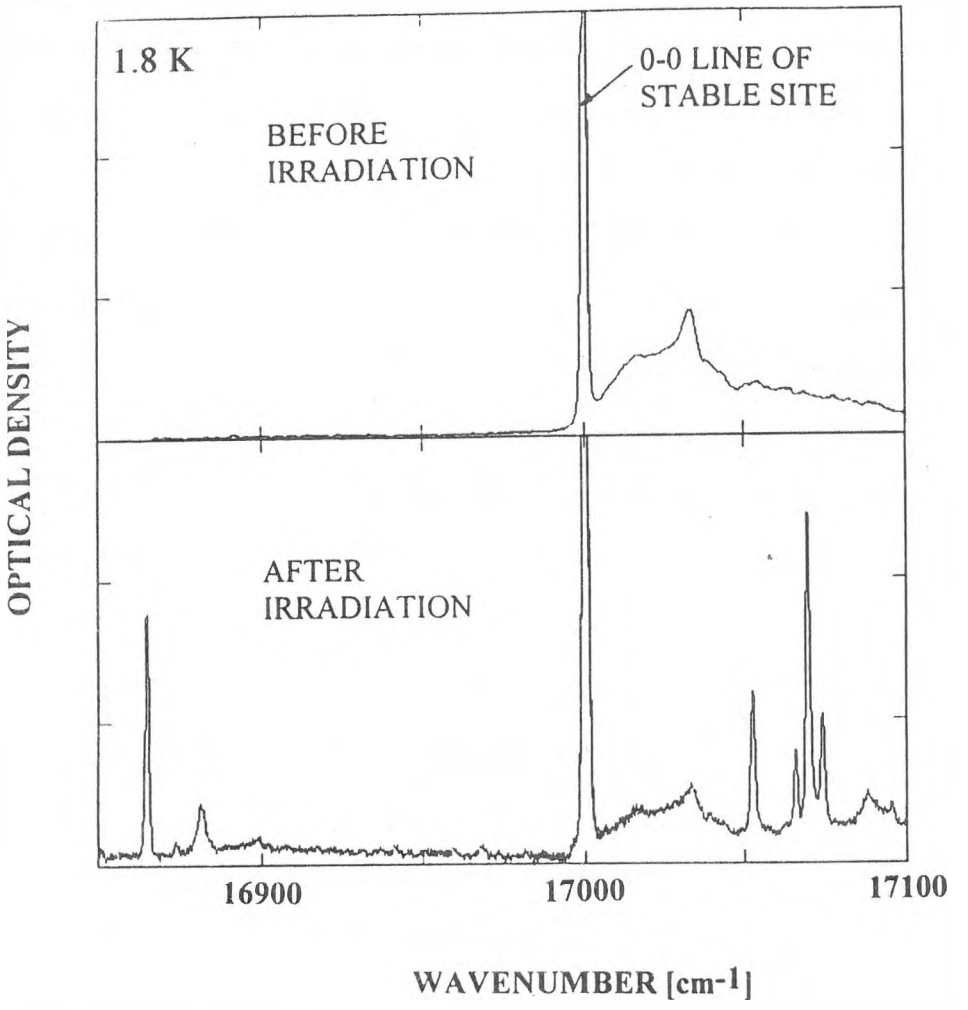

Fig. 2: Absorption in the region of electronic origin ($S_1 \leftarrow S_0$) transition of pentacene doped in single crystals of benzoic acid. **a**): spectrum of the crystal prior to irradiation, **b**): spectrum recorded after irradiation at the frequency of 0-0 line of the stable site at 16 998.3 cm^{-1}.

molecules in *altered* environment. The ground state energy of different defects site or altered environment is higher than of the stable sites but the energy differences between the different defect structures may be quite small (the transition energies ranges from 140 cm^{-1} below to 80 cm^{-1} above the transition energy of the stable site)

B. Photochemistry and relaxation in pentacene doped benzoic acid crystals.

The photoinduced mechanism involved in this systems was presented in the previous studies [6-8]. The general picture of reaction mechanism and ensuing relaxation and interconversion processes of sites is summarized in Fig. 3.

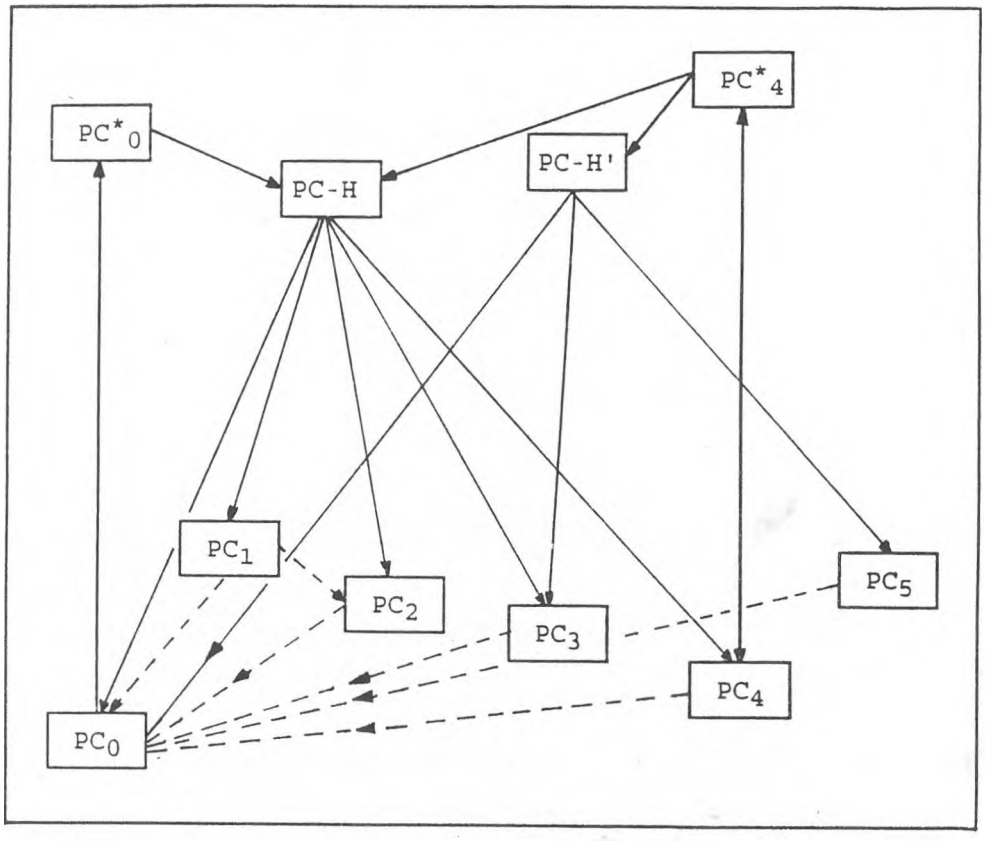

Fig. 3: Reaction scheme leading to the production of defect sites by reversible hydrogen transfer reactions. The figure also indicates photoinduced and spontaneous relaxation processes between sites.

Then, prior to irradiation the mixed crystal contains only PC in the stable site (PC_0). Electronically excited PC_0^* abstracts a hydrogen atom from the matrix giving an unstable protonated dye (PC-H). This complex dissociates rapidly into ground state and the hydrogen

atom is released back to the matrix, not necessarily in its original position (PC_0) but to a displaced or metastable site (PC_i, i=1, ..., 4). Re-excitation of PC in this metastable site (i.e. PC_4 photosite) is again followed by protonation and releasing of the proton in existing sites (PC_0 to PC_4) or new sites (PC_5). All photosites decay to the stable site, either directly either by feeding other photosites ($PC_1 \rightarrow PC_2$). In addition to relaxation directly back to original unperturbed structure, photosites can also "communicate" subsequent to light absorption or re-excitation. The photosites can be bleached by re-irradiation but in this case, the efficiency of bleaching is increased significantly (one order of magnitude or more).

The proof of reaction scheme, proposed here as mechanism leading to the defects structures, relies heavily on:

1) the differences of reactivity of *selectively deuterated PC molecules* [6, 9].

2) the isotope effect on the rate of relaxation of matrix (i.e. the acid protons of the benzoic acid dimers replaced by deuteriums).

3. PHOTOINDUCED PROTON DISORDER IN PENTACENE DOPED BENZOIC ACID CRYSTALS - A MODEL FOR DISORDERED SOLIDS

A. Results. Benzoic acid and related carboxylic acids crystallize as cyclic dimers linked by two hydrogen bonds. These dimers can rearrange via simultaneous two-proton transfer into a tautomeric structure. For a isolated dimer the potential diagram describing the tautomer is a symmetric double well. In the benzoic acid crystals the double well has been shown to be asymmetric. Thus, although a crystalline medium is involved, there is a disordered structure due to different tautomer configuration. This disorder fluctuates on a nanosecond time scale

and is perceived as static or dynamic, depending upon the intrinsic time scale of the spectroscopy that is performed.

However, a different type of disorder is created in crystal, even at 0 K, when the stable pentacene molecule embedded in crystal is irradiated. This is a *photoinduced disorder* which can be connected to the disorder pre-existing in glasses and, consequently, we propose to analyze in the terms of so-called Anderson's two-level system (TLS) [10] used in description of glasses structure.

Then, prior to irradiation, the PC-doped BA crystals at liquid helium exhibit all the properties of an ideal sustitutionally doped mixed crystal system. The replacement of BA dimers by PC molecules occurs at random (Fig. 4 (a)).

Disorder have been created in the crystal at low temperature by irradiation, so that a great variety of defect structures is produced as described above (Fig. 4 (b)).

It is this ensemble of PC molecules in a variety of defect structures that can be regarded as a disordered solid. This ensemble exhibits many of the characteristics of dye molecules doped into glass:

i) The spread of transition energies of the different defect sites is over 200 cm^{-1} (see Fig. 2 and Fig. 4 (b)). This inhomogeneous spread is comparable to site shifts observed in crystals (i. e Spols'kii matrices) or to the width of the inhomogeneous distribution observed for electronic transition of dye dissolved in glasses .

ii) The communication between different defect structures in the absence of irradiation is an example of *spectral diffusion process* which is operative in a like glass systems.

iii) The communication between different defect structures in the presence of

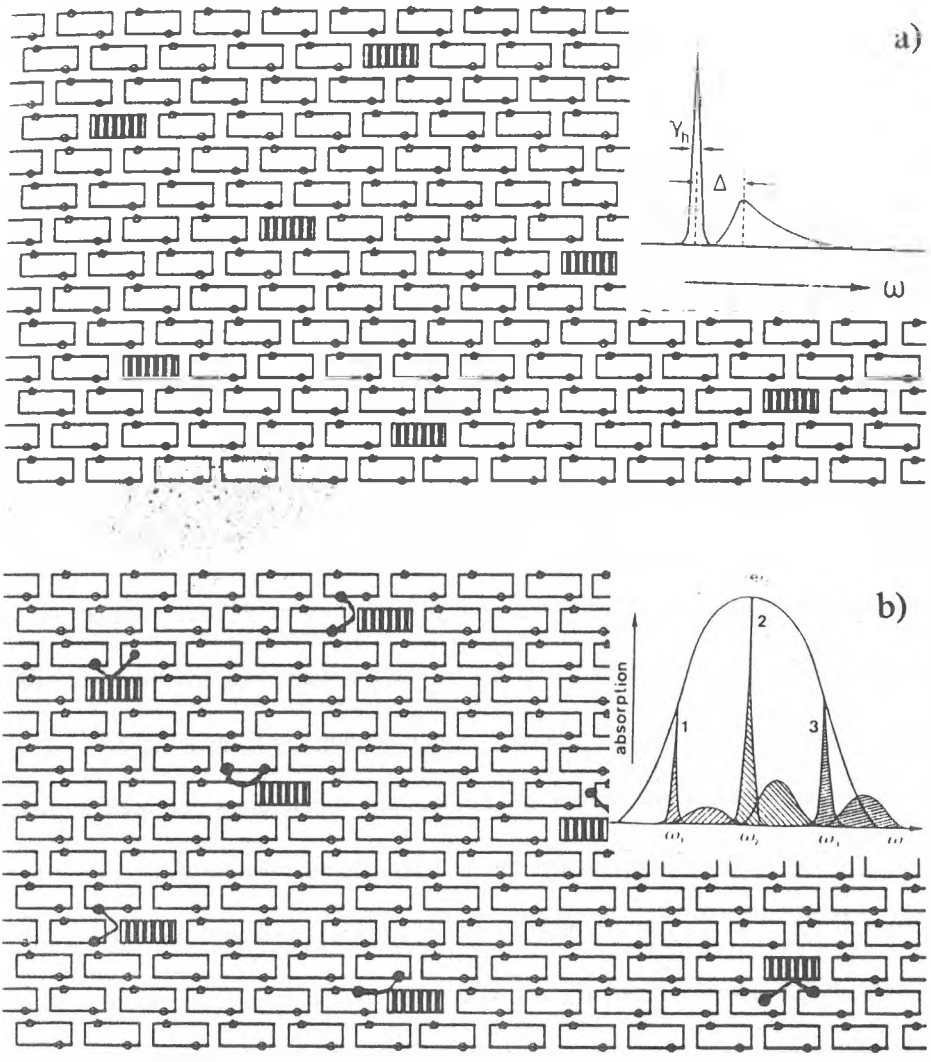

Fig. 4: **a)** Schematic representation of the stable sites of a substitutionally doped benzoic acid crystal and of the spectum prior to irradiation. The open rectangles represent benzoic acid dimers of the host where small circles indicate two acid hydrogens of a dimer, while the pentacene guests are represented by striped rectangles. **b)**: Schematic representation of the ensemble of defect structures with displaced hydrogen atoms and of the spectrum, obtained after irradiation of the sample.

irradiation can contribute to elucidating the *hole burning* and *light induce hole filling* mechanisms in amorphous materials.

The observations ii) and iii) matches, for a continuous distribution of sites as present in glass, the spectral evolution in these materials [11]. The spontaneous as well as the photoinduced communications between the photosites in PC/BA irradiated crystal are shown in Fig. 5 (a) and (b).

iv) In many regards the defect structures in a crystal is analogous to probing the distribution of dye sites in a glass by measurements on *single molecules spectroscopy,* as observed at very low doping levels [12]. In both cases the properties of each site (rates of relaxation, temperature dependence, crystal-field-induce dipole moments, etc.) are well defined and distinct, while in a glass at higher doping levels only averages of these quantities are observed.

B. Discussion. Relaxation of photoinduced perturbations in PC/BA mimics the *spectral diffusion process* which is operative in a like glass systems. Consequently, the relaxation between a photosite and the site stable or also even the communication between different defect structures observed in PC/BA can be modeled by the glass two level system model (TLS). Following Anderson's model the double-well potential is shown in Fig. 6. This double-well potential is a very simplified representation of the disordered structure around of pentacene dye. Because the state reached after irradiation is one of non-equilibrium, like the glassy state, the bulk disorder is taken into account by a "discrete" distribution of parameters Δ_i and V_i.

Ignoring the phonon assisted relaxation, the tunneling at T=0K is the unique process of relaxation. One form the tunnel states $| A >$ and $| B >$ from the two localized oscillator states (the site state and the photosite state , respectively):

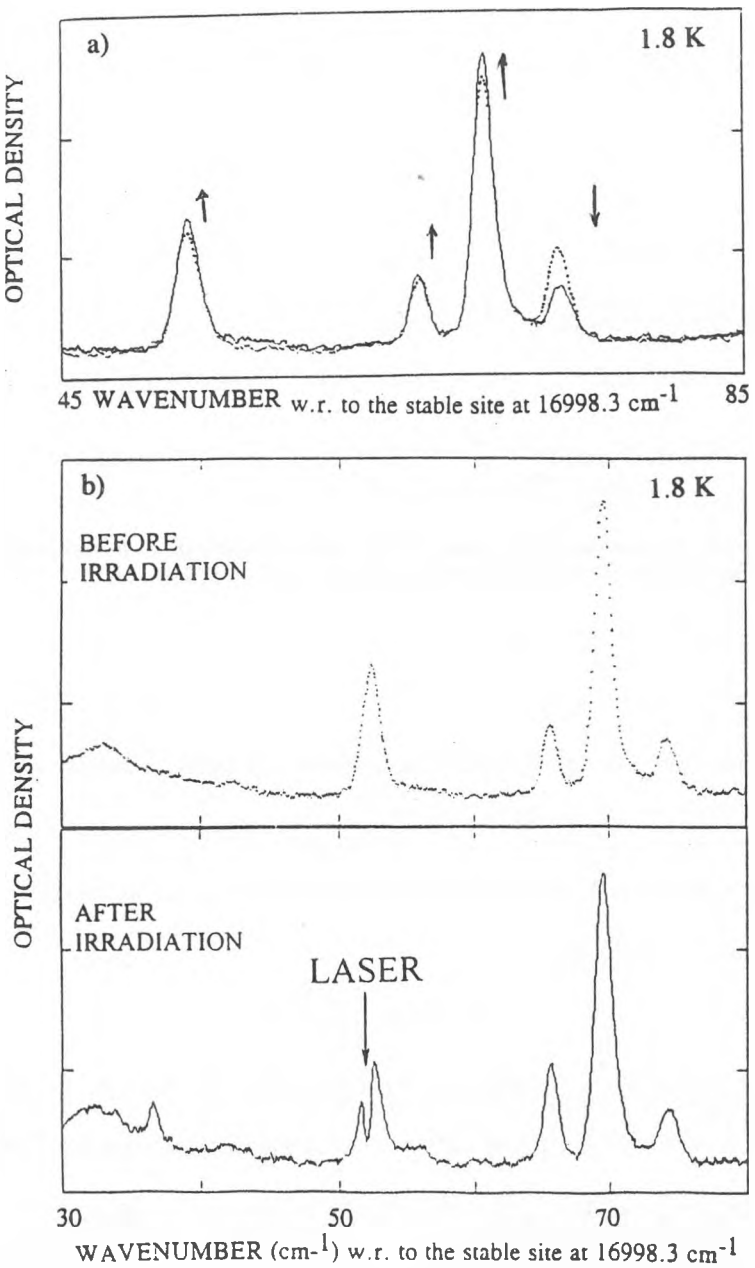

Fig. 5: **a)** Communication between different sites in the absence of light (in dark). The decay of the site at 74.3 cm^{-1} feeds the sites at 52.3 cm^{-1}, 65.7 cm^{-1} and 70.1 cm^{-1}. **b)**: Communication between different defect sites via irradiation: selective irradiation of the site at 52.3 feeds the site at 65.7 cm^{-1} and at 36.7 cm^{-1}. (All energies are relatives to the stable site: 16 998.3 cm^{-1}).

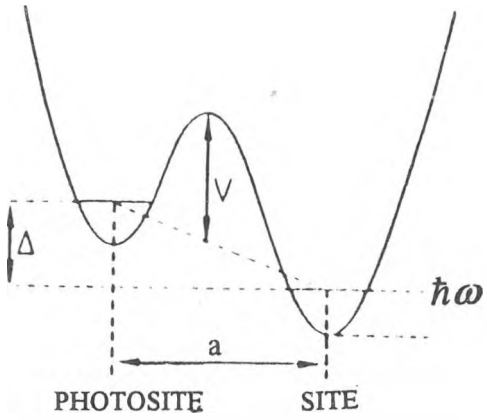

Fig. 6: A schematic representation of the double-well potential characteristic two-level systems (TLS). The relevant parameters are shown here and discussed in the text.

$$| A > = a| L_{site} > + b| R_{photosite} >$$

$$| B > = -b| L_{site} > + a| R_{photosite} > \quad (1)$$

The formal description of tunneling state can be done by one 2x2 Hamiltonian matrix:

$$H = \frac{1}{2}\begin{bmatrix} \Delta & J \\ J & -\Delta \end{bmatrix} \quad (2)$$

In the above matrix the Δ parameter characterizes the potential asymmetry and J is the tunneling frequency of the form:

$$J = \hbar\omega \exp\left(-\frac{\sigma a}{h}\sqrt{2mV}\right) \quad (3)$$

where **a** is the separation of two potential wells along the coordinate, **m** is the particle mass and **V** is the barrier height as defined in Fig. 6 The energy **ħω** is on the order of the quantum energy of a harmonic oscillator and characterize the shape of the potential.

The rate of relaxation at T=0K photosite to site is:

$$k_{12} \sim J^2 \quad (4)$$

This theoretical model allow to analysis the deuteration or isotope effect in PC/BA crystals.

Then the isotopic substitution of acid protons (H↔D) leads to the follow factor which can be measured experimentally by the timelife of photosite:

$$r_{H/D} = \frac{k_{12}(H)}{k_{12}(D)} = 2\exp\left[\frac{1.4a}{\hbar}\left(\sqrt{2m_D V_D} - \sqrt{2mV}\right)\right] \quad (5)$$

Our measurements of timelife [6] showed that the lifetime of photosites is slowed down by three and more orders of magnitude in the deuterated host, so the deuteration effects on the relaxation rates impose that $r_{H/D} > 10^4$. These large deuteration effects confirm that the defect structure are due to a rearrangement of the acid protons of the host. The tautomerization of BA dimers next to the PC guest was also invoked [13], but rejected based upon the great number (> 20) of photosites observed, the time scale of the relaxation, as well as the energy of photosites relative to the stable site (> 700 cm^{-1}). Clearly, more severe proton rearrangements, involving the rupture of hydrogen bonds or even of =O-H bonds, produced by reversible hydrogen (proton) transfer reaction between the guest and host molecules were proposed as alternative explanation [6] .

$$1\ \text{Å} \leq a \leq 2\ \text{Å}$$

and

$$r_{H/D} > 10^4$$

Consequently, assuming proton tunneling distances of a few Angstroms :

one estimates barriers heights of 1000-5000 cm^{-1} (see Fig. 7).

This is an interesting result: we learn from these experiments that the PC/BA crystal is, after irradiation, very nearly like a glass system. Especially, the result show that the barrier heights exceed considerably the barriers of the tautomerisation process (<700 cm^{-1}) and are comparable with the barrier heights given in glasses. This effect provides important insight

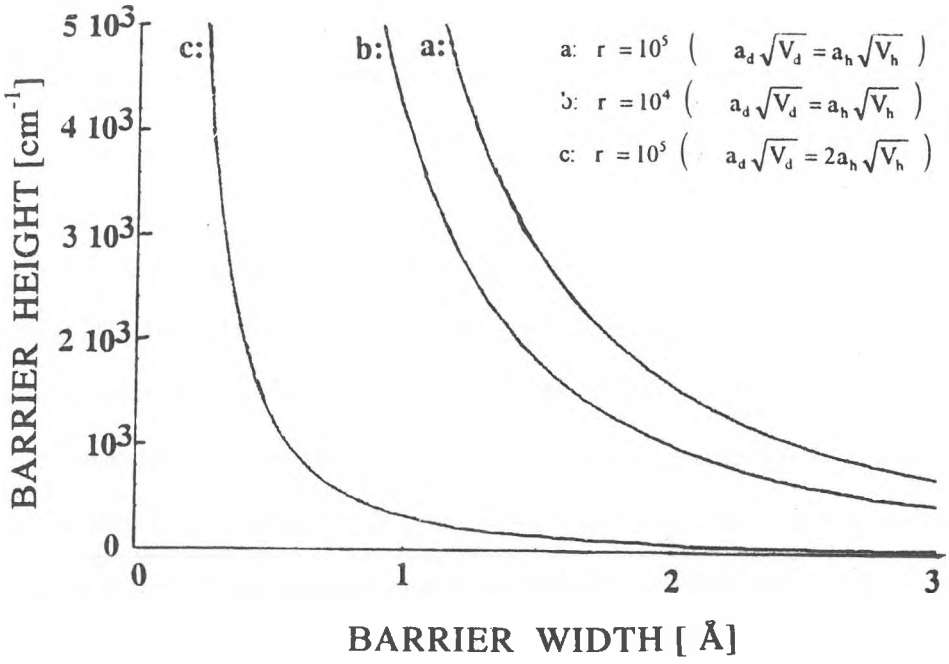

Fig. 7: Combination of barrier heigths and widths obtained from the isotope effects on the decay rates of the photosites structures.

into the distances over which hydrogen are displaced and the energy barriers separating different hydrogen arrangements.

After irradiation of PC/BA crystals, the ensemble of metastable defect sites created, exhibits properties that are characteristic of disordered solid like glass, so that this crystalline system can be used as a model of these more complicated solids.

4. Conclusions

Photoinduced hydrogen displacements, such as characterized here in PC-doped crystals, are likely to occur in many doped crystalline systems and glasses. Similar, though not as detailed, observation of such processes have been made for other dopants of BA and also for

various dopants in durene [14]. Reversible host-guest hydrogen transfer reactions could be identified in the present system as leading to the hydrogen displacements in the host environment and we propose that this mechanism is also operative in many doped glasses where such a detailed characterization is not feasible. Such a mechanism would contribute to so-called non photochemical hole burning and the light-induced hole filling processes. The proposition that the ensemble of photoinduced defects sites in PC-doped BA is representative of a dye-doped amorphous solid is supported by the observed characteristics and behavior of this ensemble at temperatures near 0 K. The possibility to investigate for the discrete defect sites the effect of deuteration on reaction rates and on the rates of relaxation is unique for the crystalline model system and such measurements cannot be done in real glasses, even using single molecule spectroscopy.

Acknowledgments. One of authors (S.A.) would like to thank H.P. Trommsdorff, A. Corval and R. Casalegno from Joseph Fourier University of Grenoble, France for their pemanently interest and encouragement during his PhD research.

REFERENCES

1. W.E. Moerner, ed., *Persistent Spectral Hole Burning: Science and Applications*, Springer, Berlin, 1988.
2. I. Zschokke, ed., Optical Spectroscopy of Glasses, D. Reidel Publishing Company, 1986.
3. G.R. Holtom, R.M. Hochstrasser, and H.P. Trommsdorff, Chem. Phys. Lett. **131**, pp.44-61, 1986.
4. A. Szabo, Phys. Rev., **B11**, 4512, 1975.
5. H.P. Trommsdorff, S. Astilean, R. Casalegno and A. Corval, Mol. Cryst. Liq. Cryst. **236,** 21, 1993.
6. S. Astilean, Ph.D. thesis: "*Transfert photoinduit de protons dans des cristaux mixtes pentacene/acid benzoique caracterisé par spectroscopie optique*", Université Joseph Fourier, Grenoble, France, 1993.
7. S. Astilean, A. Corval, R. Casalegno and H.P. Trommsdorff, J. Luminiscence, **55**, 1731, 1994.

8. R. Casalegno, A. Corval, S. Astilean and H.P. Trommsdorff, J. Luminiscence, **53**, pp.211-214, 1992.
9. S. Astilean, V. Chitta, A. Corval, R.J.D. Miller, and H.P. Trommsdorff, Chem.Phys.Lett., **219**, 95, 1994.
10. P. W. Anderson, B.J. Halperin and C.M. Varma, Philos. Mag. **25**, 1, 1972.
11. G.J. Small, in *Spectroscopy and Excitation Dynamics of Condensed Molecular Systems* ed by V.M. Agranovich and R.M. Hochstrasser, North-Holland Comp., pp.515-555, 1983.
12. M. Orrit, J. Bernard, A. Zumbusch and R.J. Personov, Chem. Phys. Lett., **196**, 595, 1992.
13. H.W.H. Lee, C.A. Walsh and M.D. Fayer, Chem. Phys. **82**, 3948, 1984.
14. B. Prass, J.P. Colpa and D.J. Stehlik, J. Chem. Phys. **88**, 191, 1981.

STUDIA UNIV. BABEŞ-BOLYAI, PHYSICA, XXXIX, 2, 1994

THE pH INFLUENCE ON THE PP VITAMIN RAMAN SPECTRA

T. ILIESCU*, S. CÎNTA*, S. ASTILEAN* and I. BRATU**

ABSTRACT. - Raman spectra of solid PP vitamin and of 10^{-1} mol/l aqueous solutions at different pH values were studied and compared. In solid state and in solution at large pH the nonprotonated species are present while in solution at low pH (<2.5) the protonated ring nitrogen atom was preponderant observed.

INTRODUCTION

PP Vitamin (Nicotinamide) has major contribution in oxidation-reduction processes of the human body. In this sense is very important to be known the changes of molecular structure of this drug at different pH values. Raman spectroscopy is a very good tool which offer the possibility to understand the molecular structure modification with the aid of vibrational analysis.

In order to understand the mechanism and the species adsorbed on silver surface when enhanced Raman spectra are obtained, a complete study of normal Raman spectra of PP vitamin in solid state and in aqueous solution at different pH values is necessary in order to establish from the vibrational analysis what kind of species are present in each case. In this sense, our work is a preliminary study about normal Raman and IR spectra of PP vitamin in solid state and solution at different pH values.

* *"Babeş-Bolyai" University, Faculty of Physics, 3400 Cluj-Napoca, Romania*

** *Institute of Isotopic and Molecular Technology, P.O.Box 700 R-3400 Cluj-Napoca, Romania*

EXPERIMENTAL

PP Vitamin was purified by many time recrystallization from ethanol-water solution until the desired melting point was obtained. The pH values of 10^{-1} mol/l aqueous solutions were adjusted by using H_2SO_4 or NaOH.

The Raman spectra were recorded on a double monochromator GDM 1000 using the 488 nm excitation line of an Ar ion laser. The laser power and the spectral slit widths are indicated on the spectra. The sample were put into a capillary glass tube and the scattered light was collected at 90° geometry without polarizer in the gathering optics. In order to avoid the plasma lines which were present especially in the Raman spectra of solid sample, the laser light was passed through a simple monochromator. Infrared spectra of solid samples were recorded with a UR 20 Carl Zeiss spectrophotometer in the 400-4000 cm^{-1} spectral range using the KBr pellet technique. All spectra have been recorded at room temperature.

RESULTS AND DISCUSSION

As the value of the pH is modified, a structure change of the PP vitamin molecule is obtained, see Fig. 1.

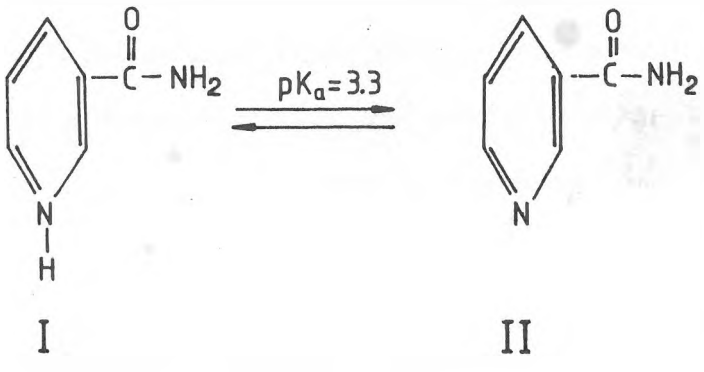

Fig.1. The structure changes of PP vitamin with the variation of pH.

The pk_a=3.3 value indicate [1] that in solution at pH values smaller than 3 3 the protonated form (I) whereas at pH larger than 3.3 neutral form (II) one are present respectively.

Fig. 2 and Fig. 3 shows the Raman and IR spectra, respectively, of solid PP vitamin. We assume that in the solid state, PP vitamin is composed by the neutral form II. In this sense we made first a vibrational analysis of the Raman spectrum for the solid state PP vitamin and then we compared this spectrum with that of the solution at different pH values.

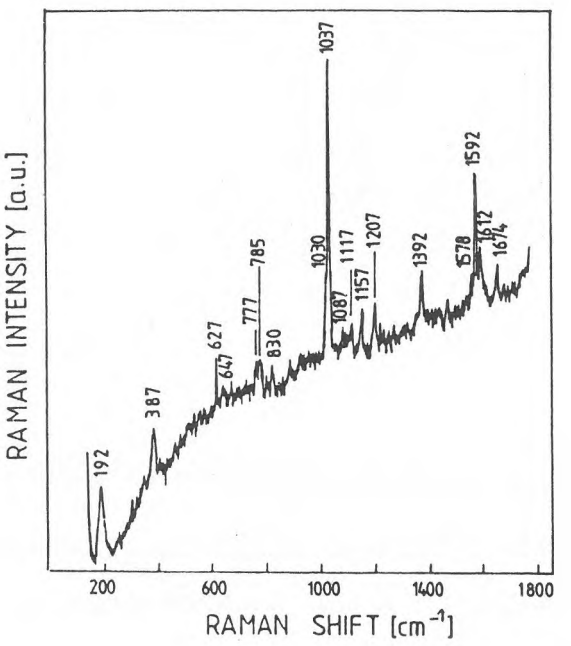

Fig.2. Raman spectra of solid PP vitamin. Excitation with 488 nm (140 mW) line of an Ar+ laser. Spectral slit width: 3 cm^{-1}.

In infrared and Raman spectra of primary amide [2,3] three type of bands are present:

Amide I - assigned to ν(C=0) stretching vibration;

Amide II - which can be assigned to the βNH_2 bending vibration;

Amide III - induced by ν(C-N) valence vibration coupled with N-H vibration. Excepting Amide I, the name "Amide" characterizes the vibration more generally that the given alternative symbols.

In benzamide (R = phenyl group) infrared frequencies for these three types of vibrations are

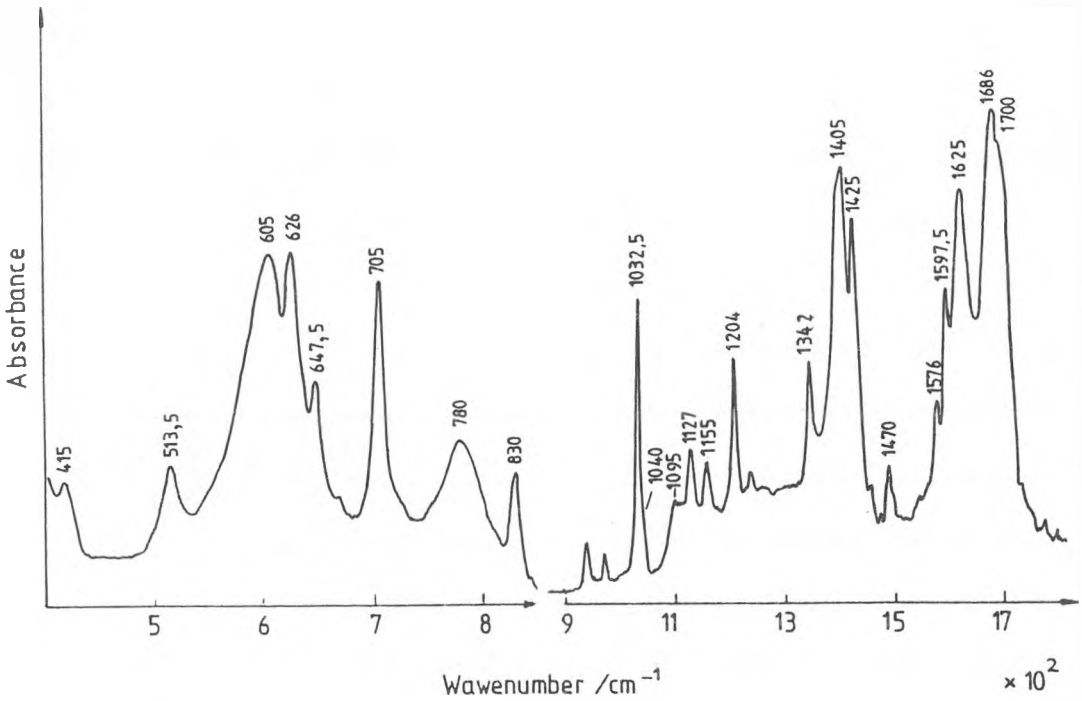

Fig. 3. IR spectrum of solid PP vitamin in the 400-1800 cm^{-1} spectral range.

centered at [3] : 1661cm^{-1} (I), 1626cm^{-1} (II) and 1404cm^{-1} (III) respectively.

By comparison with infrared and Raman spectra of benzamide and Raman spectra of nicotinic [4] and isonicotinic acids [5], in Raman spectra of solid PP vitamin (fig.2), the band at 1674 cm^{-1} can be assigned to $\nu(C = 0)$ stretching vibration (amide I); 1612 cm^{-1} to bending vibration NH_2 (amide II) and 1392cm^{-1} to ν(C-N) valence vibration coupled with N-H vibration (amide III). In infrared spectra of PP vitamin these bands are identified at 1686 cm^{-1}, 1625cm^{-1} and 1405 cm^{-1} respectively.

The strong band present in Raman spectra at 1592 cm^{-1} and the accompanying week should

at 1578 cm^{-1} can be assigned to the in plane *8a* and *8b* ring stretching vibrations, using Wilson's notation for monocyclic aromatic components[6]. Corresponding to IR data, these bands are placed at 1597cm^{-1} and 1576 cm^{-1}. For pyridine ring and in benzamide these vibrations are present at 1583cm^{-1}, 1572 cm^{-1} and 1600cm^{-1}, 1577 cm^{-1} respectively.

A very strong band at 1037 cm^{-1} with a shoulder at 1592 cm^{-1} is the most intense band in the Raman spectra of solid PP vitamin (Fig. 2).

In analogy with the spectra of monosubstituted benzene and pyridine derivatives [7], this doublet generally arises from the 12 trigonal ring "breathing" mode and 5 out-of-plane CH deformation.

In the spectral range between 1100cm^{-1} and 1500 cm^{-1} some peaks of weak intensity resulting from further in plane ring vibrations can be found at 1087cm^{-1} (*18b*), 1117 cm^{-1}, 1157 cm^{-1} (*13*) and 1207cm^{-1} (*9a*).

At low Raman shifts, two bands at 777 and 785 cm^{-1} are assigned probably to the O = C - NH_2 in plane bending vibrations; the band at 627 cm^{-1}(*6b* or (C-O)) and 387 cm^{-1}(*16b*) are also present. At very low frequencies, a band at 192 cm^{-1} is observed (Fig. 2) which can be probably due to the vibration of molecules in elementary cell of crystalline PP vitamin or the vibration of crystalline network.

In order to understand the mechanism and the species adsorbed on silver surfaces, when Enhanced Raman Scattering is observed, the changes of the molecular structure of PP vitamin at different pH values are necessary to be known. In this sense, we obtained normal Raman spectra of 10^{-4}mol/l PP vitamin water solution at different (0.5-12) pH values. For pH larger than 5.5 (this pH was obtained only by solving PP vitamin at desired

concentration) there are no substantial changes observed in the Raman spectra.

In Fig.4 we present the Raman spectra of 10^{-1}mol/l PP vitamin aqueous solution at three pH values: 0.5, 2.5 and 5.5. Depending on pH value, we can obtained in solution the proto-nated or nonprotonated form of PP vitamin (Fig 1). The protona-tion can be easily realized at pyridine ring nitrogen and proba-bly hardly at NH_2 amide group. This happens at very low pH values ($pH<<pK_a$) when PP vita-min predominantly exists as pro-tonated form [I] and at large pH as neutral form [II].

The changes observed in Raman spectra convinced us about the existence of these molecular species. As we can see from Fig.4 a meaningful change in Raman spectra at different pH values is observed only in the 1550 - 1700 cm^{-1} range in addition to the broadening and the shift of all the bands in comparison with the bands of solid PP vitamin.

In solution as in the solid state the most intense band arises from the trigonal "breathing" mode 12 at 1045 cm^{-1} accompanied by the out-of-plane 5 CH deformation at 1030 cm^{-1}. The last band rises in intensity as pH value increases (Fig. 4b and 4c). In aqueous solution saturated in nicotinic acid at pH = 12.5, when the spectrum can be associated with the nicotinated anion (nitrogen atom from pyridine ring is not protonated), only 12 mode at 1037 cm^{-1}[4] is present. In Raman spectra of solid state PP vitamin (Fig 2) two very closed bands at 777 and 787 cm^{-1}, of the same intensity, are present. The Raman spectra of solution at pH = 0.5 show only a intense band at 782 cm^{-1} and at pH = 2.5 this band appears as a shoulder (785 cm^{-1}) on the intense band at 794 cm^{-1}, while at pH = 5.5 only the intense band at 792 cm^{-1} is present.

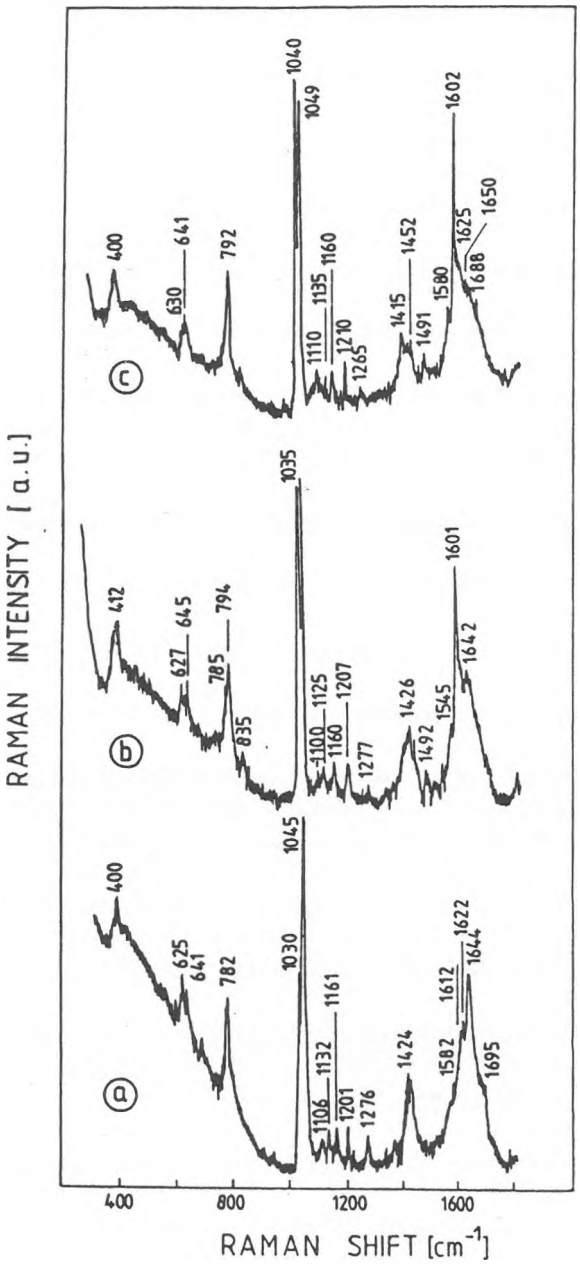

Fig.4. Raman spectra of 10^{-1} mol/l water solution of PP vitamin: a) pH = 0.5; b) pH = 2.5; c) pH = 5.5. Excitation with 488 nm (140 mW) line of an Ar+ laser. Spectral slit width: 4 cm^{-1}.

Because this band was assigned to O = C - NH_2 in plane bending vibration we assigned these changes in intensity and position either to the presence of protonated form I or to hydrogen bond in amide group

In infrared spectra of solid PP vitamin one finds a large band at 780 cm^{-1} with a shoulder at 755 cm^{-1}. The existence of this large band confirm us the presence of hydrogen bond in amide group even in solid state. At large pH values (pH > 5.5, fig. 4c) in Raman spectrum a very strong band centered on 1602 cm^{-1} is present with shoulders at 1625 cm^{-1}, 1650cm^{-1} and 1688cm^{-1} on the high wave numbers and 1580cm^{-1} on the low wave numbers. These bands are similar to the bands 1578cm^{-1}, 1592 cm^{-1}, 1612 cm^{-1} and 1674cm^{-1} observed in Raman spectrum of solid state PP vitamin (Fig.2). This is an argument that in solution at pH values larger even than 2.5 the PP vitamin exists in its neutral form (II Fig 1).

At low pH values Raman spectrum shows a different aspect in the 1500 cm^{-1}-1700cm^{-1} spectral region (Fig. 4a). A strong band at 1644 cm^{-1} is present with shoulders at 1582 cm^{-1}, 1622 cm^{-1} and 1695cm^{-1}. As can be seen from fig. 4 the decrease of pH leads to the reduction of signal intensity of the ring vibration *8a* at 1602cm^{-1}, while simultaneously a new band develops at 1644 cm^{-1} which at pH = 0.5 became very intense.

This fact reflects the structural change of the dominant species from the neutral PP vitamin (form II Fig.2) to the protonated form I ones.

In general, N - protonation of pyridine derivatives produces a wave number shift of the vibrational band *8a* [7] i.e in the case of pyridine from 1583 cm^{-1} to 1630 cm^{-1}. For nicotinic acid this wave number shift was observed from 1589 cm^{-1} (pH = 12) to 1644 cm^{-1} (pH < 4.6) and is explained by the presence of the nicotinic acid anion (nonprotonated

nitrogen ring) and zwitterion (protonated nitrogen ring).

The Amide III band present in the solid state Raman spectrum of PP vitamin at 1392 cm^{-1} is shifted in solution at 1424 cm^{-1} and is broadened. At pH = 5.5 a shoulder is developed on this band at 1452 cm^{-1}.

CONCLUSIONS

The structural transitions of PP vitamin in aqueous solution 10^{-1} mol/ l in the entire pH - range are reflected in normal Raman spectra. The protonation of the nitrogen ring can be observed from the intensity changes and the development of new Raman bands which correspond to the protonated or nonprotonated species.

REFERENCES

1. I.Grecu, E.Curea - Identificarea substantelor medicamentoase, Ed. Dacia Cluj-Napoca, 1980, p.260.
2. M.Avram, Gh.D. Mateescu- Spectroscopia în infrarosu. Aplicatii în chimia organică. Ed. Tehnica Bucuresti 1966, p.498.
3. G.Varsanyi - Assignments for vibrational spectra of 700 Benzenol Derivatives. Akademiaikiado, Budapest 1973, vol. I, p.72.
4. J.Barthelmes, G. Pofahl, W.Plieth . Ber. Bunsenges. Phys. Chem. 96 1055 (1992)
5. S.M. Park, K.Kim, M.S.Kim. J.Molec. Structure 328 169 (1994).
6. E.Spinner. J. Phys. Chem. 92 3379 (1988).
7. F.R. Dollish, W.G.Fateley, F.F.Bentley - Characteristic Raman Frequencies of Organic Components, John Willey and Sons, London, Sidney, Toronto 1974.

STUDIA UNIV. BABEŞ-BOLYAI, PHYSICA, XXXIX, 2, 1994

SPIN FLUCTUATIONS IN $(U_{1-x}La_x)Al_4$ SYSTEMS

Ileana LUPŞA*, P. LUCACI* and Mihaela DANCIU**

ABSTRACT. - The structural and magnetic properties of $(U_{1-x}La_x)Al_4$ systems were studied. The compounds having $x \leq 0.6$ and over a certain temperature a Curie Weiss type behaviour obey. The negative paramagnetic Curie temperatures and the effective magnetic moments values indicate the presence of the spin fluctuations. For $x=0.8$ a Pauli paramagnetism is evidenced. As lanthanum content is increasing a quenching of spin fluctuations and their supression are observated. The magnetic measurements are correlated with the structural data.

I. INTRODUCTION

UAl_4 was evidenced as a spin fluctuations system. It presents a maximum in the thermal susceptibility dependence at ~200K and over a certain temperature (400K) a Curie Weiss type paramagnetism is followed [1]. The crystalline symmetry is a orthorombohedral one [2].

We intend to study the influence of uranium substitution on the magnetic and structural behaviour and for that we replaced uranium by a nonmagnetic rare earth element, lanthanum.

The $LaAl_4$ crystalline structure is of two types: at lower temperatures an orthorombohedral one and for T>915°C a tetragonal symmetry is observed [3].

The magnetic measurements on $(U_{1-x}La_x)Al_4$ systems were performed in the 77-600K temperature range. The X ray analyses confirmed the uniphase presence of these compounds for $x \leq 0.6$. For $x=0.8$ a mixture of two phases (orthorombohedral and tetragonal) are present.

* *Technical University, 3400 Cluj-Napoca, Romania*

** *"Babeş-Bolyai" University, Faculty of Physics, 3400 Cluj-Napoca, Romania*

II.EXPERIMENTAL RESULTS

The samples were melted in an arc furnace in purified argon atmosphere and were thermally treated in vacuum at 700K for one week.

The susceptibility of UAl_4 presents over 400K a Curie Weiss dependence with the paramagnetic Curie temperature -850K and the effective magnetic moment due to uranium atom 3.9 μ_B.

The thermal dependence of the reciprocal susceptibility for the systems $(U_{1-x}La_x)Al_4$ is presented in figure 1. For $x \leq 0.6$ and temperature higher than 100K the magnetic behaviour may be described by a modified Curie Weiss law: $\chi=\chi_o+C(T-\theta)^{-1}$. C represents the Curie constants, θ is the paramagnetic Curie temperature and by χ_o is denoted the temperature independent susceptibility term. For x=0.8 the system is a Pauli paramagnet having $\chi=4\ 10^{-4}$ emu/fu. $LaAl_4$ from our measurements is diamagnetic with $\chi=-5\ 10^{-5}$emu/fu.

We present in figure 2 the composition dependence of C values and the effective magnetic moments μ_{eff}. The molar Curie constants are decreasing as the lanthanum content is greater to the value 0.245 emu K/fu for x=0.6. The μ_{eff} values are almost linearly decreasing from 3.9 μ_B (corresponding to uranium free ion in UAl_4) to 1.85 μ_B for x=0.6.

The θ values are negative as it is seen from figure 3 and are linearly decreasing in absolute magnitude from 850K (for UAl_4) to 300K for x=0.6.

χ_o values presented in figure 2 are increasing as the lanthanum content becomes greater reaching the value $4\ 10^{-4}$ emu/fu for x=0.8. A similar magnetic behaviour was previously reported for $(U_{1-x}La_x)Al_2$ systems [4].

The X ray analyses show that the systems having $x \leq 0.6$ are uniphase compounds with

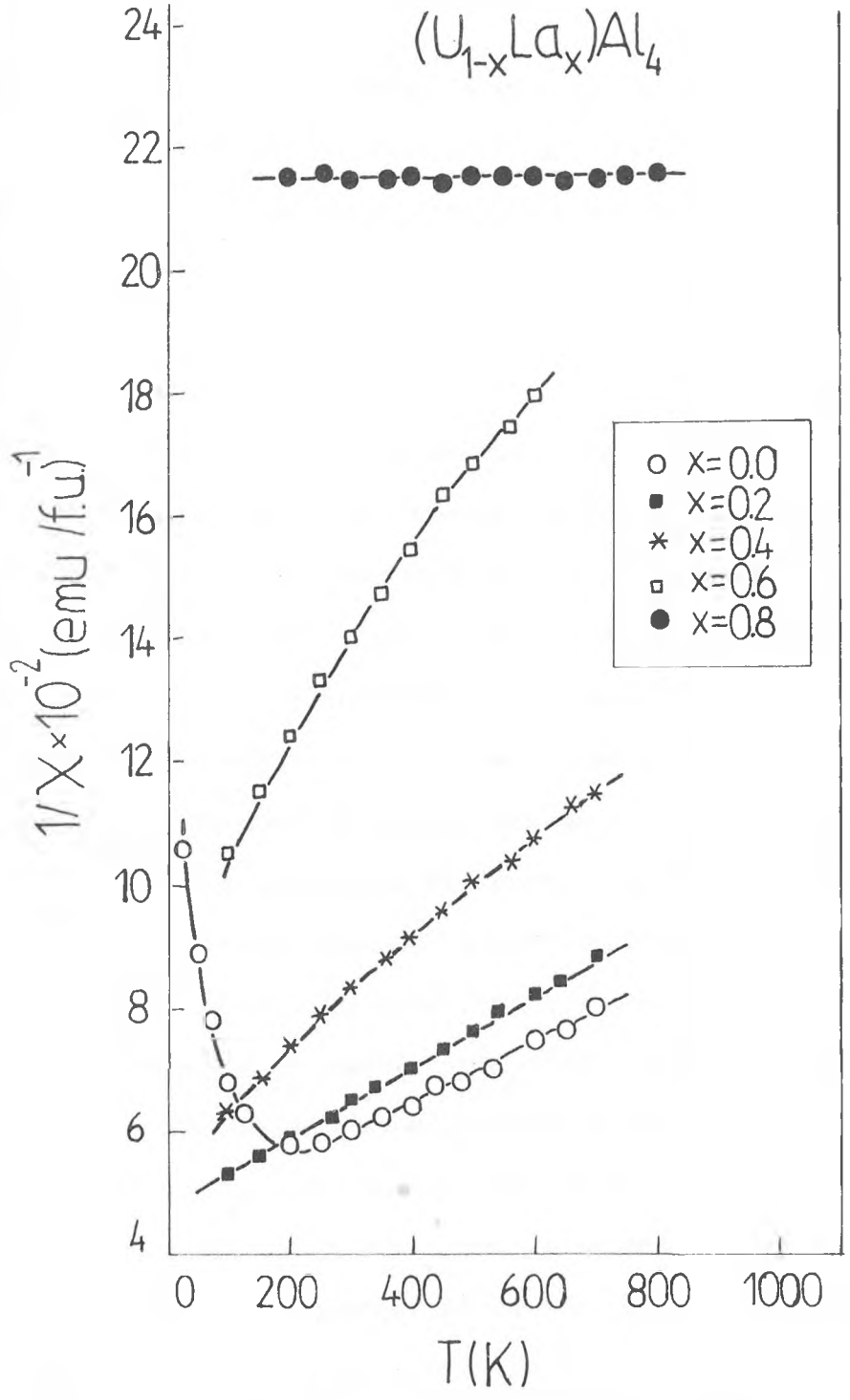

Fig 1. The thermal dependence of the reciprocal susceptibility values for $(U_{1-x}La_x)Al_4$ systems.

the orthorombohedral symmetry. The crystalline constants are slowly modified of that of UAl_4. The system $U_{0.2}La_{0.8}Al_4$ is a mixture of two phases : orthorombohedral and tetragonal, the last one being predominant. The lattice constants of the tetragonal phase are little different of that of $LaAl_4$.

III. DISCUSSION

The magnetic moment value, corresponding to uranium free ion, and the negative paramagnetic Curie temperature for UAl_4 as well as the maximum in the susceptibility support the presence of spin fluctuations. The Curie Weiss behaviour over a certain temperature T^*=400K justifies the interpretation of the magnetic properties in the terms of the selfconsistent renormalization theory of spin fluctuations (SCR) [5,6,7]. In this model the wave number dependent susceptibility χ_q has a large enhancement due to electron-electron interaction only for small q and is temperature dependent. The average amplitude of local spin fluctuations $< S_{loc}^2 >= 3k_B T \sum_q \chi_q$ is increasing as the temperature is increasing up to T^*. At T^* the amplitude reaches an upper limit determined by the charge neutrality condition.

The pseudobinary systems $(U_{1-x}La_x)Al_4$ having $x \leq 0.6$ show a Curie Weiss type paramagnetism ,in all studied temperature range, with negative paramagnetic temperatures. The effective magnetic moments and the absolute values of θ are decreasing when uranium is substituted by lanthanum. The Pauli term is increasing as x is greater. All these facts support the presence and gradual quenching of spin fluctuations when the substitution element is increasing. The system with x=0.8 is a Pauli paramagnet.Its magnetic behaviour is correlated with the change evidenced in the crystalline structure from orthorombohedral (the

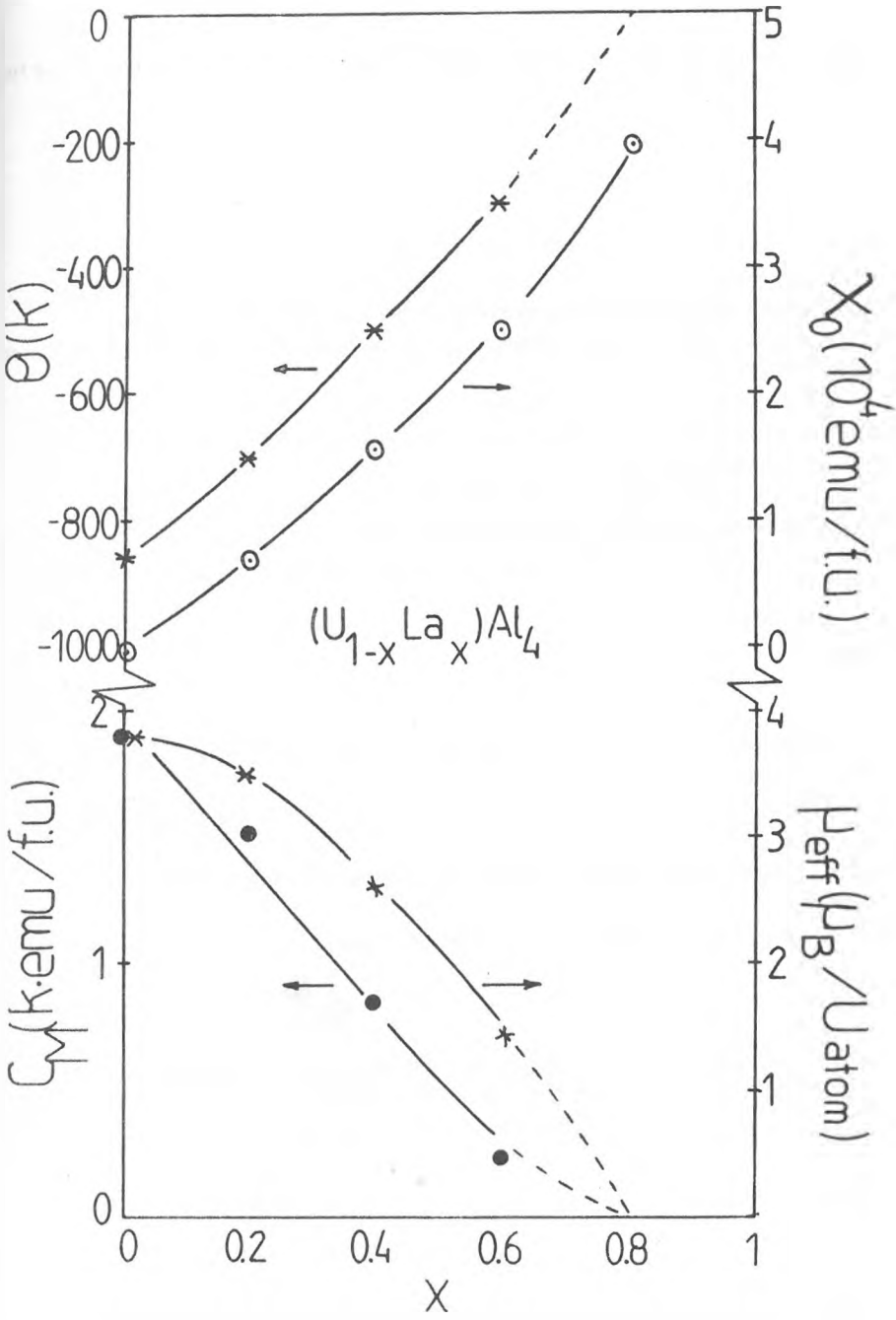

Fig 2. The composition dependence of C,μ_{eff},θ and χ_o values for $(U_{1-x}La_x)Al_4$ compounds.

UAl_4 symmetry) to tetragonal (the $LaAl_4$ structure) $U_{0.2}La_{0.8}Al_4$ being a mixture of these two phases.

REFERENCES

1. E.Burzo, P.Lucaci and I.Lupsa, J.Magn.Magn.Mater. **140-144** (1995) 1413.
2. V.Sechovsky and L.Havela in E.P.Wohlfarthn and K.H.J.Buschow "Handbook of Ferromagnetic Materials",vol.4 (1988).
3. K.H.J.Buschow, Philips Res.Rep.**20** (1965) 337.
4. E.Burzo,P.Lucaci and E.Gratz,Solid State Commun.**72** 4 (1989) 397.
4. T.Moriya,J.Magn.Magn.Mater.**14** (1979) 1.
5. T.Moriya and A.Kawabata,J.Phys.Soc.Jpn.**34** (1973) 635.
6. E.Burzo and R.Lemaire,Solid State Commun.**84** (1992) 1145.

STUDIA UNIV. BABEŞ-BOLYAI, PHYSICA, XXXIX, 2, 1994

PHYSICAL PROPERTIES OF $(U_{1-x}Y_x)Al_3$ SYSTEMS

P. LUCACI and I. LUPSA*

ABSTRACT. - The magnetic properties of $(U_{1-x}Y_x)Al_3$ compounds in the temperature range 77-600K are reported. A spin fluctuations type behaviour is evidenced. When uranium is replaced by ytrium a gradual quenching of spin fluctuations is observed.

I. INTRODUCTION

The magnetic properties of UAl_3 compound evidence the presence of a maximum in the thermal dependence of the susceptibility (at 140K) and over a certain temperature T^* (at 250K) a Curie Weiss type behaviour. The paramagnetic Curie temperature is negative (-450K) and the effective magnetic moment ($3.6\mu_B$) is that of uranium free ion. These features prove the presence of spin fluctuations [1]. The crystalline structure of this compound is a cubic one of $AuCu_3$ type [2].

The YAl_3 is a Pauli paramagnet having a hexagonal symmetry of $SnNi_3$ type with lattice parameters a=6.276Å and c=4.528Å below a certain temperature and at higher ones it becomes rhombohedral [3].

We present the magnetic and structural properties of pseudobinary UAl_3 based compounds obtained replacing uranium by ytrium.

II. EXPERIMENTAL RESULTS

The samples were melted in an arc furnace in a purified argon atmosphere. In order to ensure good homogeneity the samples were remelted several times. The alloys were treated

* *Technical University, 3400 Cluj-Napoca, Romania*

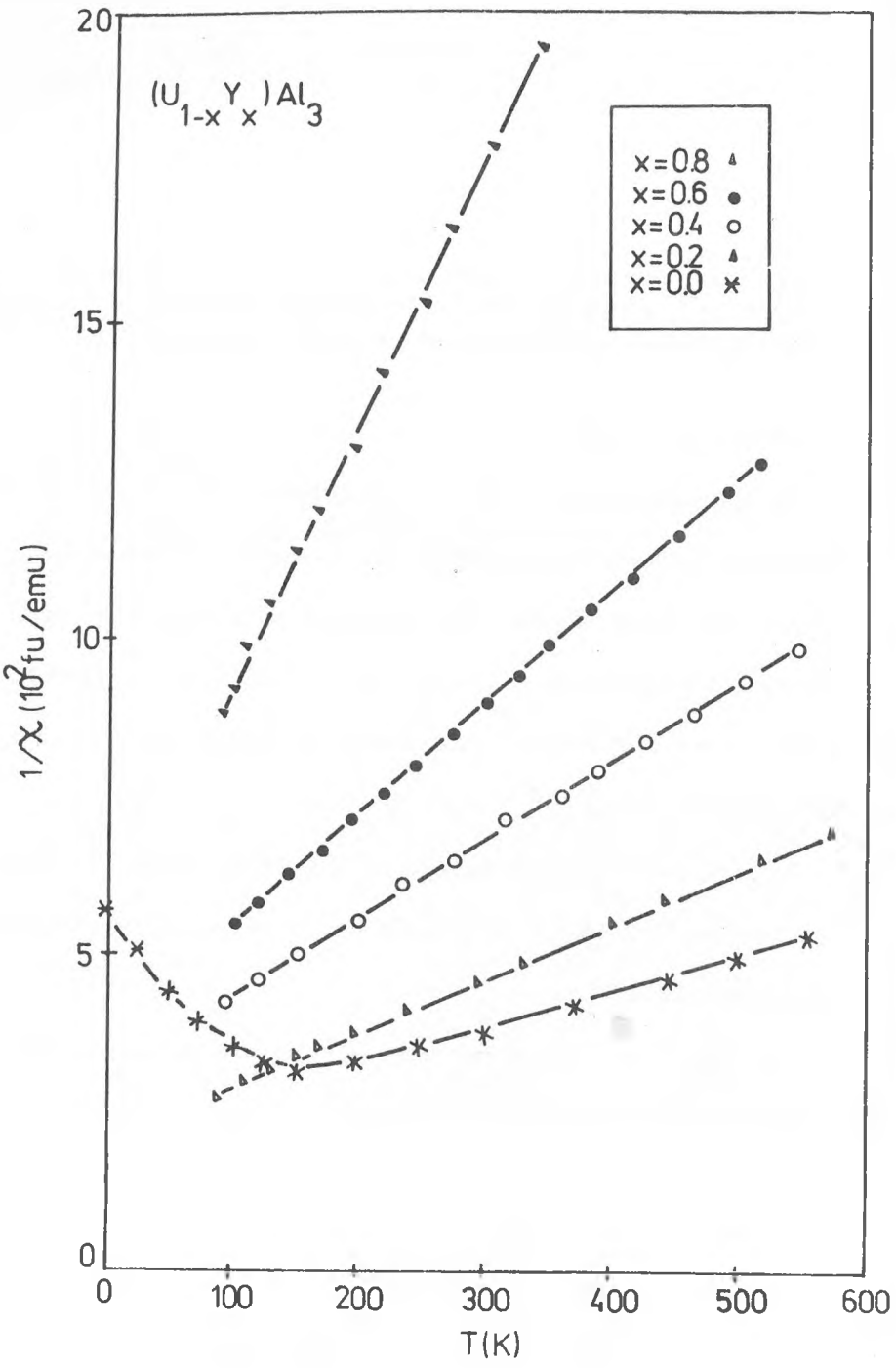

Fig. 1. The thermal dependence of the reciprocal susceptibility for $(U_{1-x}Y_x)Al_3$ systems.

in vacuum at 800K for one week. The magnetic measurements were performed in the temperature range 77-600K.

The X-ray analyses indicate the presence of uniphase for all compounds except that with x=0.6. The compounds having x<0.6 have a cubic symmetry like UAl_3. The lattice constants vary from 4.23 Å (for x=0) to 4.35Å indicating a slow increasing as the ytrium content is greater. The systems having x≥ 0.8 are hexagonal indexated. The lattice parameters for x=0.8 are a=6.21Å and c=4.53Å a little lower that those of YAl_3. The system $(U_{0.4}Y_{0.6})Al_3$ is a mixture of cubic and hexagonal symmetries, cubic phase being predominant.

The thermal variation of reciprocal susceptibilities for $(U_{1-x}Y_x)Al_3$ compounds are presented in Figure 1. For UAl_3 over 250K and for the pseudobinary alloys in all measured temperature range a Curie-Weiss type behaviour is evidenced.

In accord with this law: $\chi = C/(T-\theta)$ we determined the molar Curie constants C, the paramagnetic Curie temperatures θ and the effective magnetic moments μ_{eff}.

The composition dependence of C,θ and μ_{eff} values are presented in Figure 2. The molar Curie constants are decreasing as uranium is substituted by ytrium. The effective magnetic moments are almost linearly decreasing as ytrium content is increasing. The paramagnetic Curie temperatures are negative and their absolute magnitudes are decreasing from 450K linearly to zero value corresponding to YAl_3.

III. DISCUSSION

The presence of spin fluctuations in UAl_3 and the compounds $(U_{1-x}Y_x)Al_3$ for x≤0.8 is supported by the negative

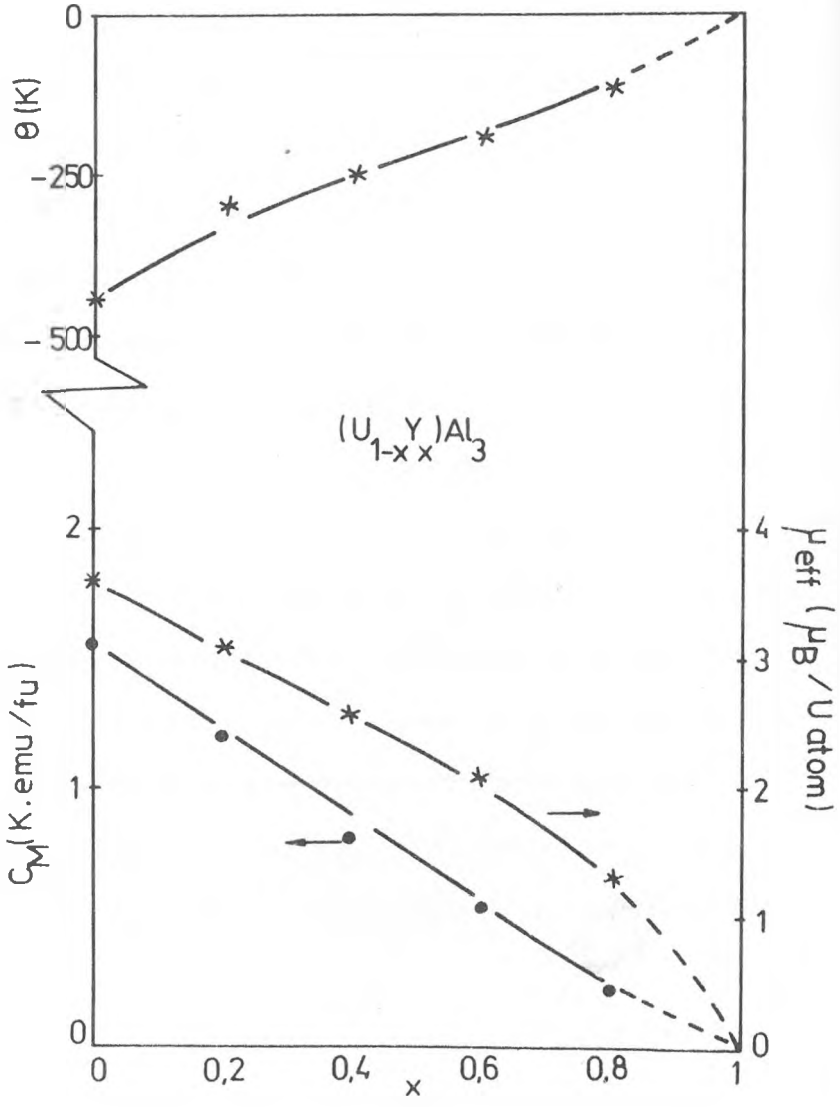

Fig.2. The composition dependence of C, μ_{eff} and θ values for $(U_{1-x}Y_x)Al_3$ compounds

values for the paramagnetic Curie temperatures. The effective magnetic moments are decreasing from the value of uranium free ion $3.62\mu_B$ (for x=0). YAl_3 being Pauli paramagnet we attribute the magnetic moments in these studied compounds only to uranium atoms. The decreasing of these μ_{eff} values as well as the decreasing of $|\theta|$ values indicate the gradual quenching of spin fluctuations.

The magnetic behaviour of $(U_{1-x}Y_x)Al_3$ systems may be discussed in the selfconsistent renormalization (SCR) theory of spin fluctuations [4,5,6] In this model the wave number dependent susceptibility χ_q has for small q large enhancement in its value. This is due to electron-electron interactions and the temperature variation of χ_q is significant only for small q. The average amplitude of local spin fluctuations $\langle S_{loc}^2 \rangle = 3k_B T \sum_q \chi_q$ is a temperature increasing quantity becoming constant over a certain temperature T^*. Over T^* a Curie-Weiss paramagnetism is evidenced, the systems behave as if having a local magnetic moments. For UAl_3 [1] the T^* value is 250K and for $0.2 \leq x \leq 0.8$ T^* probably becomes lower than 77K in all measured temperature range a Curie-Weiss type paramagnetism being evidenced.

REFERENCES

1. I.Lupsa, P.Lucaci and E.Burzo, J.Alloys and Comp. **204** (1994) 247
2. A.E.Dwight, Acta Crytallogr.B24 (1968) 1395
3. D.M.Bailey, Acta Crystallogr.**23** (1967) 729
4. T.Moriya, J.Magn.Magn.Mater.**14** (1979) 1
5. T.Moriya and A.Kawabata,J.Phys.Soc.Jpn.**34** (1973) 639
6. E.Burzo and R.Lemaire,Solid State Commun.**84** (1992) 1145

STUDIA UNIV. BABEŞ-BOLYAI, PHYSICA, XXXIX, 2, 1994

THE EFFECT OF Cu SUBSTITUTION BY Zn IN THE 108 K PHASE OF THE (BiPb)-Sr-Ca-Cu-O SUPERCONDUCTOR

A.V. POP*, D. CIURCHEA*, I.I. GERU, V.G. KANTSER***, L.A. KONOPKO**, V.I. GERU*** and Gh. ILONCA***

ABSTRACT. - The effect of the Cu substitution by Zn in the (BiPb)-(SrBa)-Ca-Cu-O superconductor was studied by resistivity measurements. The paraconductivity showed a 2D to 3D cross-over temperature in all samples. The decrease in the critical transition temperature along with the increase in the residual resistivity are discussed in relation with the disorder produced by the Zn ions in the CuO_2 planes.

1. INTRODUCTION. Since the discovery of high T_c superconductivity in the Bi-Sr-Ca-Cu-O system [1,2], many investigations have been devoted to the understanding of the role of Cu. Superconductivity with 110 K transition temperature has been associated with the n=3 polytype of the ideal composition $Bi_2Sr_2Ca_2Cu_3O_{10+\delta}$ [3], referred to as "2223" phase. The substitution of Bi by Pb up to 40% promoted and stabilized the 110 K phase [4]. The reduction of to less than 3+ of the Bi valency reveals that the BiO layers act as hole reservoirs [5]. The insertion of oxygen in the Bi layers causes lattice distortions producing holes in the Cu-O sheets and an incommensurate modulation of the structure [6,7].

The study of the Cu substitution by other ions is hoped to reveal the roles of the Cu-O sheets and Cu-O pyramids on the high T_c superconductivity. In such ceramic systems the competition of the intra- and intergrain conductivity is strongly temperature dependent [8-10].

By contrast to the classical superconductors, the high T_c ceramic superconductors have

* *"Babeş-Bolyai" University, Faculty of Physics, 3400 Cluj-Napoca, Romania*

** *Moldova State Univesity, Faculty of Physics, 277014 Chişinău, R. Moldova*

*** *Institute of Applied Physics, 277028 Chişinău, R. Moldova*

a 2D dimensionality conduction and short coherence length which enhance the thermal fluctuations of the order parameter near the critical temperature [12] The 2D to 3D cross-over temperature depends on the Cu-O interlayer coupling. These features are used in this paper to report the effect of the Cu substitution by Zn in the 108 K stabilized superconducting phase, by using resistance measurements in a small concentration range up to 5% at.

2. EXPERIMENTAL. The compound $(Bi_{1.8}Pb_{0.46})(Sr_{1.88})Ca_{2.06}(Cu_{1-x}Zn_x)_3O_y$ with x=0.00, 0.02 and 0.05 were sinthesised by solid state reaction of appropriate amounts of the metal oxides and carbonates of 99.99% purity. The Sr substitution by Ba was used to induce the reduction of the modulation period and to increase the T_c onset [11].

Appropriate amounts of Bi_2O_3, PbO, $SrCO_3$, $CaCO_3$, CuO and ZnO were mixed in an agate mortar and calcined at 800°C for 36 hours. The calcinated powder was pressed into pellets and sintered at 850°C for 250 hours in air with one intermediate grinding. These pellets were cooled down to room temperature with a rate of 32°C/hour. The test specimens were rectangularly machined from the pellets.

The qualitative X-Ray diffraction analysis performed with a DRON-2 equipment confirmed the presence of a single "2223" phase in the samples x=0 and 90% "2223" in the x=0.02 and x=0.05 samples respectively. The doped samples presented traces of the "2212" and "2201" superconducting phases.

The electrical resistance was measured by the standard four-lead technique between 77 and 290 K.

3. RESULTS AND DISCUSSION. The temperature dependence of the electrical resistance R(T) for the samples x=0.00, 0.02 and x=0.05 are shown in Fig. 1.-3. In the 180-290 K range, these samples are characterized by a linear temperature dependence of the resistance:

$$R_n = R(0) + a*T \tag{1}$$

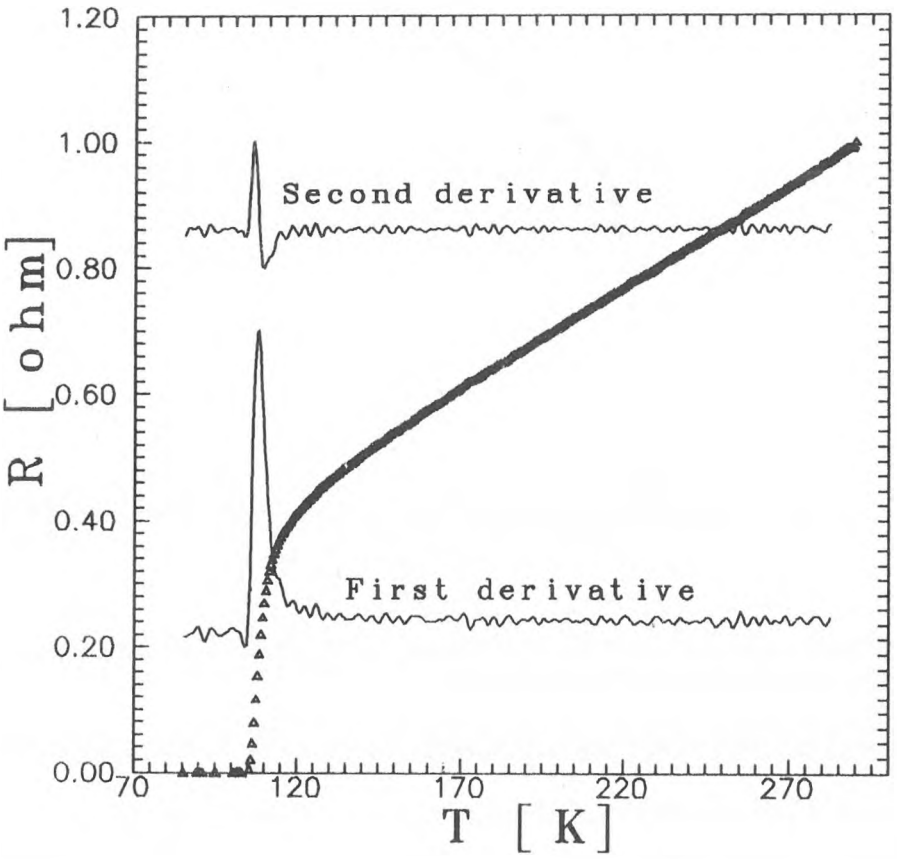

Fig. 1. The temperature dependence of the electrical resistance data for the x=0.00 sample, along with the first and second derivatives of the smoothed data.

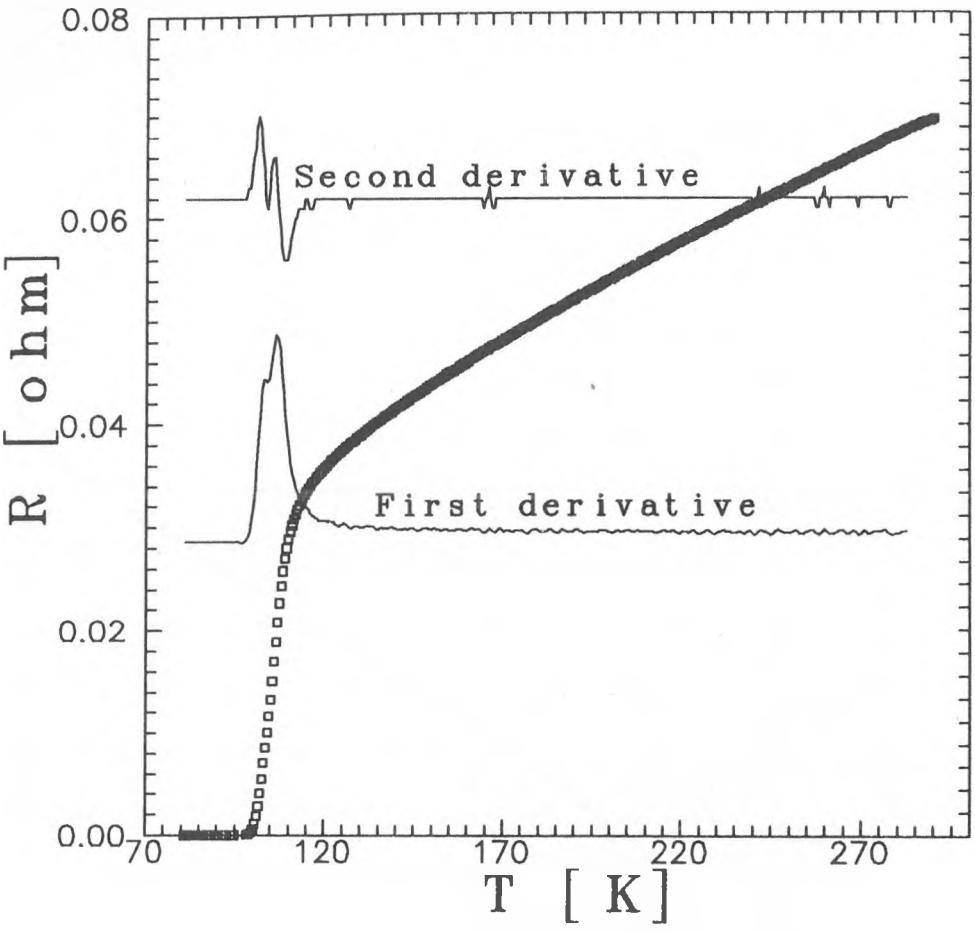

Fig. 2. The temperature dependence of the electrical resistance data for the x=0.02 sample, along with the first and second derivatives of the smoothed data.

this relation was used to find the residual resistivity obtained from R(0) and the slope $d\rho/dT$, see Table 1. One may observe an increase in the residual resistivity with increasing Zn doping level.

The critical transition temperature, $T_c=T_{cm}$, was obtained as the maximum observed in the first derivative of $dR(T)/dT$ [16], presented along with R(T) in Fig. 1.-3. The second

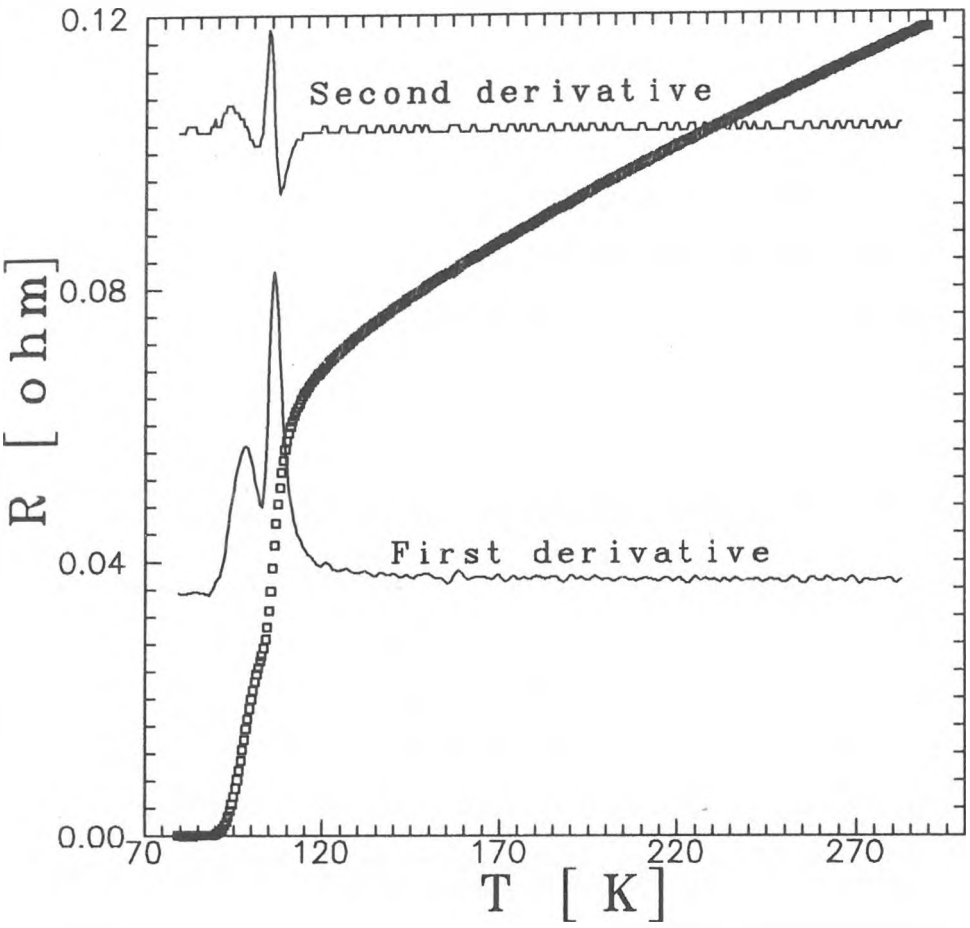

Fig. 3. The temperature dependence of the electrical resistance data for the x=0.05 sample, along with the first and second derivatives of the smoothed data.

derivative is plotted also in order to reveal if many T_c are to be considered in the analysis. Smoothing of the data was performed by using the 'moving average method' [14,15]. Two critical transition temperatures may be used to describe the Zn doped samples, see fig. 2.-3. and Table 1. The lower T_c decreases with increasing Zn content suggesting a substitution of Cu by Zn in the pyramidal coordinated Cu sites in the CuO_2 planes. This T_c is characteristic

for the 2223 and not for the 2212 superconductors which have a maximum T_c lower than 92 K. Since the maximum of the derivative yields a T_c=106.5 K, one may assume that Zn mainly substituted Cu in the CuO_2 sheets.

The extrapolation at low temperature of the linear dependence of $R_n(T)$ yielding the normal state resistivity in the fluctuation regime [12] was computer processed. From the measured electrical resistance R and from R_n the excess conductivity $\Delta\sigma/\sigma$ was calculated, with $\sigma_0=1/\rho(290)$, were $\rho(290)$=1.5, 1.6 and 1.8 mΩcm in the samples with x=0.00,0.02 and 0.05 respectively. The analysis of the excess conductivity above the mean transition temperature T_{cm} has been performed in the framework of the Lawrence-Doniach model [13]. In this model the excess conductivity, based on the Aslamasov-Larkin fluctuation [14] taking place in the superconducting layers coupled by Josephson tunneling is :

$$\frac{\Delta\sigma}{\sigma_0} = \frac{A(2D)}{\sqrt{\varepsilon(\varepsilon+4J)}} \qquad (2)$$

Table 1. The values of $\rho(0)$ and $a=d\rho/dT$ obtained from the linear fit,the coupling constant J and the critical temperatures T_{cm} obtained in the experiments.

Sample M	$\rho(0)$ [10^{-4} Ω·cm]	$d\rho/dT$ [10^{-6} Ω·cm/K]	J	T_{cm} [K]
0.00 Zn	0.866	4.387	0.004	108
0.02 Zn	4.41	3.863	0.0196	106.5 103.0
0.05 Zn	6.82	3.792	0.0208	106.5 98.5

where $\rho_0=\rho(290)$, $\varepsilon = (T-T_{cm})/T_{cm}$ is the reduced temperature, J is the coupling constant between the superconducting layers and A(2D) is the temperature independent amplitude:

$$A(2D) = \frac{\rho_0 e^2}{16\hbar d} \tag{3}$$

where d is the interlayer spacing. The conduction in the "2223" copper oxides has an intrinsic two-dimensional (2D) character in the Cu-O **a-b** planes and an accentuated variability along the **c** axis. For the weak coupling between the CuO_2 blocks (J<<1), Eq. (2). reduces to the 2D term:

$$\frac{\Delta\sigma}{\sigma_0} = A(2D)\varepsilon^{-1} \tag{4}$$

In order to test the 2D behavior, the log-log plot of the experimental $\Delta\sigma/\sigma_0$ vs. ε for the x=0.02 and x=0.05 samples are shown in Fig. 4. and Fig. 5. respectively.

Within the $-5.4 < \ln(\varepsilon) < -1.1$ a clearly T_{c0} cross-over temperature can be observed in the sample with x=0, with a 2D dimensionality above, and a 3D dimensionality below (Fig. 4.). This feature was further confirmed by fitting $\Delta\sigma/\sigma_0$ to the AL term. A 3D behavior with λ=-0.51 and a 2D behavior with λ=-1.1 were obtained in the temperatures ranges $-5.4 < \ln(\varepsilon) < -4.3$ and $-4.2 < \ln(\varepsilon) < -1.91$ respectively. From the slope change in Fig. 4. and by taking an interlayer spacing d=37 Å for $T_0=T_{cm}(1+4J)$ in the Lawrence-Doniach model [13], a cross-over temperature T_0 = 109.6 K and a coupling constant J=0.004 were found yielding the coherence length $\xi_c(0)$=2.3 Å. For the Zn doped samples the range of the 3D regime increases and an obvious enhancement of this regime may be observed in Fig. 4 and Fig. 5. for x=0.02 and x=0.05 The lines in these figures are of 0.5 slope. In Fig. 5. one may additionally observe that by choosing the lower T_c as reference for ε the 3D regime persists although its range diminishes.

The interlayer coupling constant $0.004<J<0.021$ obtained in the frame of the

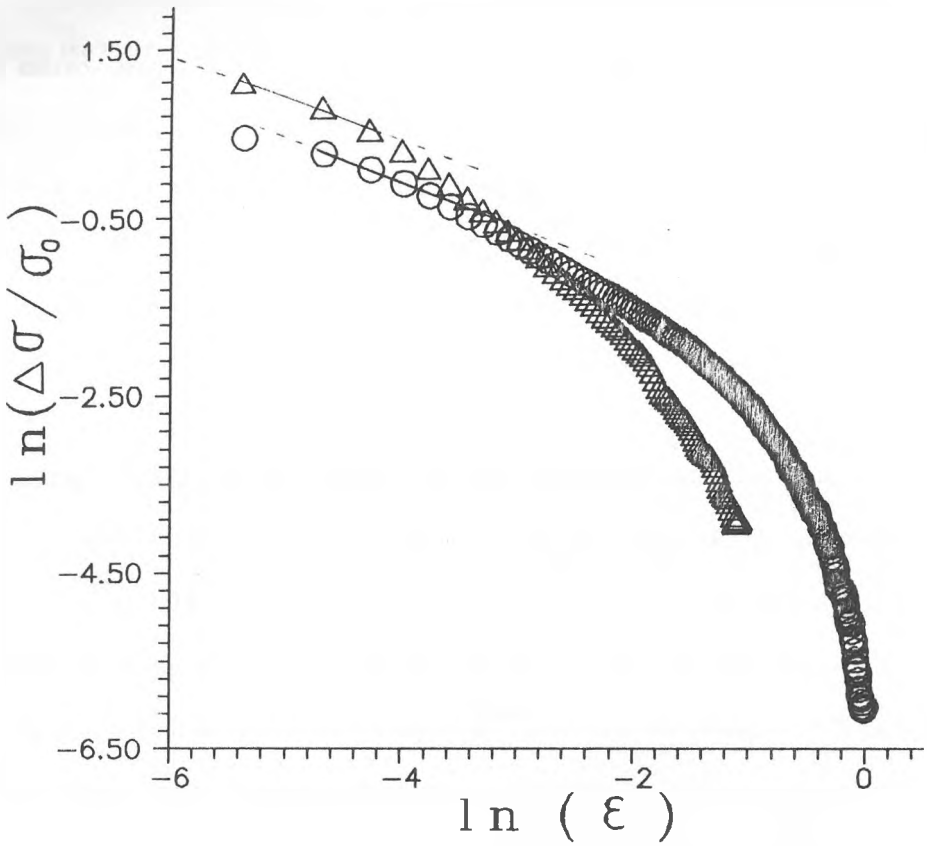

Fig. 4. The log-log plot of the normalized excess conductivity $\Delta\sigma/\sigma_0$ vs. the reduced temperature (ε) for the x=0.00 sample (triangles) and for the x=0.02 sample (circles).

Lawrence-Doniach model indicates a 2D nature of the conductivity in our system.

Comparatively to the present study, in similar Cr doped samples [17] only a 2D character was evidenced. The presence of phase mixtures (2223 and 2212) does not yield relevant contributions to the excess conductivity around 110 K [18]. In our system, the range of the 3D regime is increased by the Zn content. A similar result was reported in the "123" system [19].

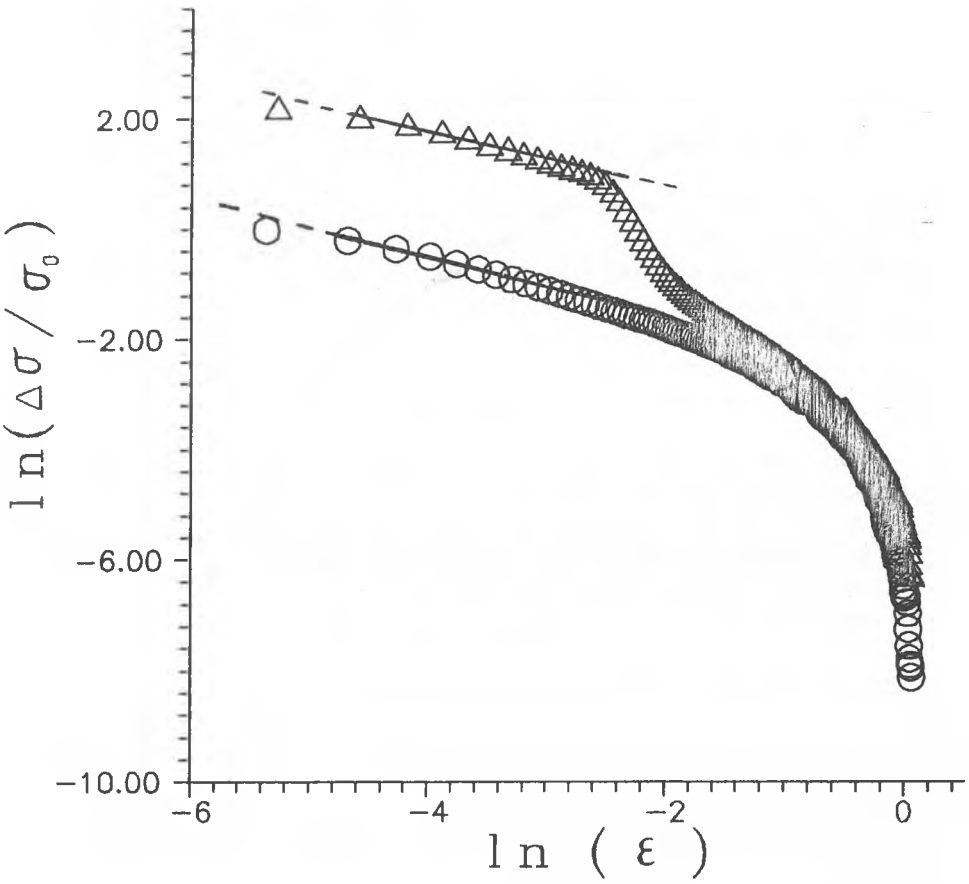

Fig. 5. The log-log plot of the normalized excess conductivity $\Delta\sigma/\sigma_0$ vs. ε for the x=0.05 sample by taking T_c=106.5 K (•) and T_c=98.5 K (▲).

4. **CONCLUSIONS**. The stabilization of the 108 K phase and the increase of $T_c(R=0)$ were obtained by the partial substitution of Bi by Pb. The Cu substitution by Zn in the concentration range $0.0<x<0.05$ was performed without a dramatic decrease of T_c.

In the Zn doped samples, the analysis of the derivative of the resistance evidenced that many T_c may be considered.

The Cu substitution by Zn was observed to induce an increase in the residual resistivity and a decrease of the lower critical transition temperature suggesting a substitution in the pyramidal sites of Cu in the CuO_2 planes.

Above the fluctuation region, a linear dependence of the electrical resistivity versus temperature was found. A cross-over temperature delimiting the 2D and 3D regimes is observed for x=0 and for the other Zn doped samples also.

REFERENCES

[1]. C. Michel, M. Hervieu, M.M. Borel, A. Grandin, F. Deslandes, J. Provost and B. Raveau, 1987,Z. Phys. **B68**, 421.

[2]. H. Maeda, Y. Tanaka, M. Fukutomi and T. Asano, 1988, Jpn. J. Appl. Phys. Lett. **27**, L209.

[3]. H.W. Zandbergen, Y.K. Huang, M.J.V. Menden, J.N. Li,K. Kadowaki, A.A. Menovsky, G. van Tendeloo and S. Amelinckx, 1988, Nature **332**,620.

[4]. H.K. Liu, S.X. Dou, N. Savvides, J.P. Zhou,N.X. Tan, A.J. Bourdillon and C.C. Sorrell, 1988, Physica **C157**, 93.

[5]. S.N. Green, Y. Mei, A.E. Manzi and H.L. Luo, 1989, J. Appl. Phys. **66**, 3703.

[6]. Y. Le Page, W.R. McKinnon, J.M. Tarascon and P.Barboux, 1989, Phys. Rev. **B40**, 6810.

[7]. J. Ren, M.H. Whangho, J.M. Tarascon, Y. Le Page, W.R. McKinnon and C.C. Torardi, 1988, Physica **C151**, 501.

[8]. J. Halbritter, 1992, J. Appl. Phys. **71**, 339.

[9]. H.Natsume, T. Kishimoto, H. Enomoto, J.S. Shin,Y. Takano, N. Mori and H. Ozaki, 1991, Jpn. J. Appl. Phys. **30**, L461.

[10]. E. Ozdas and T. Firat, 1993, Phys. Rev **B48**, 9754.

[11]. M. Zhiquiang, F. Chenggao, S. Lei, Y. Zhen, Y. Li and W. Yu, 1993, Phys. Rev **B48**, 14427.

[12]. S. Labdi, S. Megtert and H. Raffy, 1993, Solid St. Commun. **85**, 491.

[13]. W.E. Lawrence and S. Doniach, 1970, Proc. of the 12-th Int. Conf. on Low Temp. Phys., Kyoto, 361.

[14]. A. Savitzky and M.Y.E. Golay, 1964, Analyt. Chem **36**, 1627.

[15]. D. Ciurchea and V. Chiş, 1995, "Prelucrarea Datelor Experimentale", Ed. Univ. "Babeş-Bolyai", Cluj-Napoca.

[16]. S.N. Bahtia and C.P. Dhard, 1994, Phys. Rev **B49**, 12206.

[17]. A.V. Pop, Gh. Ilonca, D. Ciurchea, V. Pop, L.A. Konopko, I.I. Geru, M. Todică and V. Ioncu, 1995, Int. J. of Modern Physics **B6**, 695.

[18]. H Sanchez, A. Marino, 1994, Physica **C235-240**, 1941.

[19]. S.N. Bahtia, C.P. Dhard, 1994, Physica **C235-240**, 1449.

STUDIA UNIV BABEŞ-BOLYAI, PHYSICA, XXXIX, 2, 1994

ELASTIC ANISOTROPY IN THE TEXTURED ZIRCALOY-4 NUCLEAR FUEL SHEATHING

D. CIURCHEA*, A.V. POP*, A. DINU, I. FURTUNĂ**, M. TODICĂ*, V. CHIŞ*, S. MASCA* and F.I. AVRAM***

ABSTRACT. - The anisotropy of the elastic moduli in textured Zircaloy is quantitatively performed by using the formalism of the irreducible representations of rotations. The modelling is performed for the cold worked, recrystallized and β transformed textures which are significant for the temperature transients texture changes. The main modifications in the texture do not appear in the principal directions but at the polar angle 45°, in the tangential direction for the usual texture and in the axial direction for the β transformed texture.

1. INTRODUCTION. Zircaloy-4 is a Zr based alloy developed for the thermal reactors as the main structural metal mainly due to its small neutron capture section. The anisotropy of the Zircaloy nuclear fuel sheathing may strongly impede the in-reactor performance of the fuel both by the radial precipitation of the hydrides and by anisotropic mechanical deformation [1]. Since the early experiments it was felt that the texture strongly affects the mechanical properties. Unfortunately the measurement of the elastic moduli is the only property which may be formulated on a crystallographic basis while the other mechanical tests have only an empirical justification. Therefore we shall present a method of calculating the anisotropy of the elastic moduli in textured Zircaloy in the frame of the irreducible representations of rotations [2,3]. Although this task was approached by others [4-8], in this paper the number of textures and the service temperatures considered practically cover the current design necessities.

* *"Babeş-Bolyai" University, Faculty of Physics, 3400 Cluj-Napoca, Romania*

** *Institute for Nuclear Research, 0300 Piteşti, Romania*

2. THEORY. The texture is defined as a reproductible preferred orientation of a mechanically processed polycrystalline material. The Bunge-Roe formalism [2,3] targets to quantitatively describe the texture as a rotation problem. It assumes that one may imaginarily rotate the crystallites until a single crystal is obtained. The operations will then be described by the Orientation Distribution Function (ODF), which is a series expansion after the irreductible representations of rotations, the generalized spherical harmonics $D_l^{mn}(\phi_1,\Phi,\phi_2)$:

$$f(g)=\sum_{l=0}^{\infty}\sum_{m=-l}^{+l}\sum_{n=-l}^{+l} C_l^{mn}\cdot D_l^{mn}(\phi_1,\Phi,\phi_2) \tag{1}$$

where (ϕ_1,Φ,ϕ_2) are the Euler angles. This function may not be directly measured and therefore one may use an equivalent representation, the Axes Distribution Function, $A(\vec{h},\vec{y})$:

$$A(\vec{h},\vec{y})=\sum_{l=0}^{\infty}\sum_{\mu=-l}^{+l}\sum_{\beta=-l}^{+l}\frac{C_l^{\mu\beta}}{2\cdot l+1}\cdot K_{lR}^{\beta}(\vec{h})K_{lD}^{\mu}(\vec{y}) \tag{2}$$

Vector $\vec{h}$ will describe the orientation of a macroscopic direction in the reciprocal space, while $\vec{y}$ will describe the orientation of a pole in the direct space. The symmetry of the specimen and of the crystal yields restrictions on the series expansion, i.e. l=0(2), μ=-l(2), β=-l(6).

A pole figure measured by the method of Schulz will stand for the (hkl) X-Ray Diffraction peak $\vec{h}_i$ and may be written as:

$$!P_{\vec{h}_i}(\vec{y})=\sum_{l=0(2)}^{\infty}\sum_{\mu=-l(2)}^{+l} F_l^{\mu}\cdot K_{lD}^{\mu}(\vec{y}) \tag{3}$$

where $\vec{y}$ = (Φ,ϕ_1) and F_l^{μ} are the Bunge coefficients of the pole figure:

$$F_l^{\mu}(\vec{h}_i) = \sum_{\beta=-l(6)}^{+l}\frac{C_l^{\mu\beta}}{2l+1}\cdot K_{lR}^{\beta}(\vec{h}_i) \tag{4}$$

For a textured polycrystal, a microscopic property described in the reciprocal space after the Φ and ϕ_2 angles as :

$$E(\bar{h})=\sum_{l=0(2)}^{\infty}\sum_{\beta=-l(6)}^{+l} e_l^{\beta}\cdot K_{lR}^{\beta}(\bar{h})$$

will have in the direct space the form [2]:

$$E(\bar{y})=\sum_{l=0(2)}^{\infty}\sum_{\mu=-l(2)}^{+l} \bar{e}_l^{\mu}\cdot K_{lD}^{\mu}(\Phi,\phi_1) \qquad (5)$$

where the $\bar{e}$ coefficients are given by:

$$\bar{e}_l^{\mu}=\frac{1}{2l+1}\sum_{\beta=-l(6)}^{+l} C_l^{\mu\beta}\cdot e_l^{\beta} \qquad (6)$$

3. EXPERIMENTAL. The samples were chemically thinned to 0.03-0.05 mm in an acid mixture oh HNO_3 and HF. At this thickness, flattening of the specimen does not produce plastic deformation and the thickness is uniform. Cold worked, recrystallized and beta transformed samples were considered. The (0002),(10.0),(10.1) and (11.0) pole figures were measured for each specimen.

The preferred orientation was measured by reflection with a Philips texture device PW 1078/00 by the Schulz technique [11,12] following a spiral with a pitch per rotation of specimen of 5°. The data were collected on a computer and corrected for defocalization by division to a random sample. Numerical smoothing of the random sample allowed the extension of the reflection range up to 87° in the tilt angle. The pole figures for the specimens considered are presented in Fig 1-2

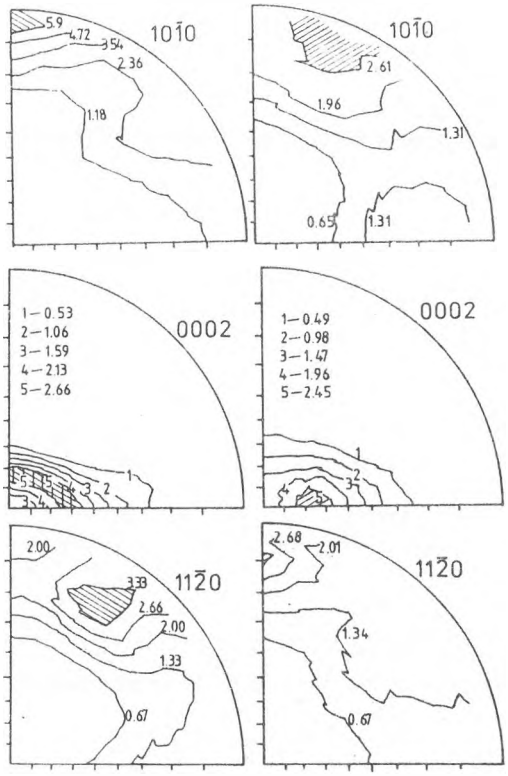

Fig. 1. The measured pole figures of the cold worked (left) and recrystallized (right) specimens [11].

4. RESULTS AND DISCUSSION. For the elastic coefficients of textured Zircaloy we start from the stress-strain tensorial expression, written for the hexagonal crystal in the rectangular axial(A) tangential(T) radial(R) frame [5]:

$$\begin{Vmatrix} \varepsilon_R \\ \varepsilon_T \\ \varepsilon_A \\ \varepsilon_{TA} \\ \varepsilon_{AR} \\ \varepsilon_{RT} \end{Vmatrix} = \begin{Vmatrix} S_{11} & S_{12} & S_{13} & 0 & 0 & 0 \\ S_{12} & S_{22} & S_{23} & 0 & 0 & 0 \\ S_{13} & S_{23} & S_{33} & 0 & 0 & 0 \\ 0 & 0 & 0 & S_{44} & 0 & 0 \\ 0 & 0 & 0 & 0 & S_{55} & 0 \\ 0 & 0 & 0 & 0 & 0 & S_{66} \end{Vmatrix} \cdot \begin{Vmatrix} \sigma_R \\ \sigma_T \\ \sigma_A \\ \sigma_{TA} \\ \sigma_{AR} \\ \sigma_{RT} \end{Vmatrix} \qquad (7)$$

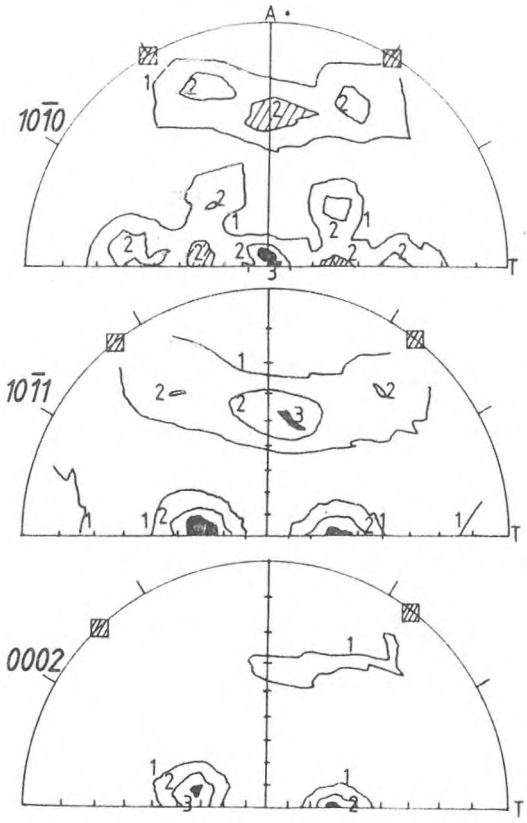

Fig. 2. The pole figures of the Zircaloy-4 tube after the α-β-α phase transformation [12].

where the compliance elastic moduli of the single crystal, S_{ij}, may be conveniently taken as those measured by Fisher and Renken [9,10] in single crystal zirconium. We have fitted these data to the following polynomial temperature dependencies:

$S_{11}(T) = 9{,}855 + 0{,}00104*T - 0{,}61*10^{-5}*T^2 + 2*10^{-8}*T^3$ [10^{-12} m²/N]

$S_{13}(T) = -2{,}391 + 9{,}11*10^{-12}*T + 1{,}1*10^{-6}*T^2$ [10^{-12} m²/N]

$S_{12}(T) = -3{,}797 + 9{,}27*10^{-3}\ T + 7{,}51*10^{-6}*T^2 + 2*10^{-3}*T$ [10^{-12} m²/N]

$S_{33}(T) = 7{,}925 + 2{,}26*10^{-3}*T + 1{,}52*10^{-6}T^2$ [10^{-12} m²/N]

$S_{44}(T) = 30{,}874 + 0{,}0157*T + 4{,}39*10^{-6}*T^2 + 1*10^{-8}*T^3$ [10^{-12} m²/N]

where T is taken in Celsius degrees

By rotations one obtains:

$$S'_{11} = S_{11}\cdot\sin^4\Phi + S_{33}\cdot\cos^4\Phi + (2S_{13} + S_{44})\cdot\sin^2\Phi\cdot\cos^2\Phi$$

$$S'_{22} = A\cdot\sin^4\Phi\cdot\cos^4\phi_1 + (2S_{13} + S_{44} - 2S_{13})\cdot\sin^2\Phi\cdot\cos\phi_1 + S_{11}$$

$$S'_{33} = A\cdot\sin^4\Phi\cdot\sin^4\phi_1 + (2S_{13} + S_{44} - 2S_{11})\sin^2\Phi\cdot\sin\phi_1 + S_{11}$$

$$S'_{12} = A\cdot\cos^2\Phi\cdot\sin^2\Phi\cdot\cos^2\phi_1 + B\cdot(\cos^2\Phi + \sin^2\Phi\cdot\cos^2\phi_1) + S_{12}$$

$$S'_{13} = A\cdot\cos^2\Phi\cdot\sin^2\Phi\cdot\sin^2\phi_1 + B\cdot(\cos^2\Phi + \sin^2\Phi\cdot\sin^2\phi_1) + S_{12}$$

$$S'_{23} = A\cdot\sin^4\Phi\cdot\sin^4\phi_1 + B\cdot\sin^2\Phi + S_{12}$$

$$S'_{44} = 4\cdot A\cdot\sin^4\Phi\cdot\sin^2\phi_1\cdot\cos^2\phi_1 + 2\cdot(S_{11} - S_{12})\cdot\cos^2\Phi + S_{44}\cdot\sin^2\Phi$$

$$S'_{55} = 4\cdot A\cos^2\Phi\cdot\sin^2\Phi\cdot\sin^2\phi_1 + (2S_{11} - 2S_{12} - S_{44})\cdot\sin^2\Phi\cdot\cos^2\phi + S_{44}$$

$$S'_{66} = 4\cdot A\cdot\cos^2\Phi\cdot\sin^2\Phi\cdot\cos^2\phi_1 + (2S_{11} - 2S_{12} - S_{44})\cdot\sin^2\Phi\cdot\sin^2\phi_1 + S_{66}$$

where

$$A = S_{11} - 2S_{13} + S_{33} - S_{44}$$

$$B = S_{13} - S_{12}$$

By using for averaging the Axes Distribution Function one may obtain the spatial variation of the elastic moduli for the textured sample. For example for the form:

$$s = A + B\cdot\cos^2\Phi + C\cdot\cos^4\Phi \tag{8}$$

one obtains :

$$S(\Phi,\phi) = (A + B/3 + C/5) + \sqrt{1/250}\left(\frac{40}{35} * C\right) +$$
$$+\left(\frac{4}{3} * B\right)\cdot(C_2^{00}K_2^0 + C_2^{20}K_2^0) + \tag{9}$$
$$+\frac{8}{9}\cdot\frac{C}{105}\sqrt{2\pi}\cdot(C_4^{00}K_4^0 + C_4^{20}K_4^2 + C_4^{40}K_4^4)$$

Here for simplicity we have written $K_l^m = K_l^m(\Phi,\phi_1)$.

The Bunge-Roe formalism implies the calculation of the Bunge coefficients of the pole

figure

$$F_l^m(\vec{H}_i) = \int_0^{\frac{\pi}{2}}\int_0^{2\pi} P_{\vec{H}_i}(\Phi,\phi_1)\cdot K_l^{*m}((\Phi,\phi_1)\cdot\sin\Phi\, d\Phi\, d\phi_1 \tag{10}$$

where

$$P_{\vec{H}_i}(\Phi,\phi_1) = \frac{I_{\vec{H}_i}(\Phi,\phi_1)/I_0(\Phi)}{\int_0^{\frac{\pi}{2}}\int_0^{2\pi} I_{\vec{H}_i}(\Phi,\phi_1)/I_0(\Phi))\cdot\sin\Phi\, d\Phi\, d\phi_1} \tag{11}$$

$I(\Phi,\phi_1)$ is the measured intensity and $I_0(\Phi)$ is the intensity for the random sample.

One may simplify the calculation of the integral by taking:

$$X_{km} = \int_0^{\frac{\pi}{2}}\int_0^{2\pi} P_{\vec{H}_i}(\Phi,\phi_1)*\sin\Phi\cdot\cos k\Phi\cdot\cos(m\phi_1)\, d\Phi\, d\phi_1 \tag{12a}$$

$$Y_{km} = \int_0^{\frac{\pi}{2}}\int_0^{2\pi} P_{\vec{H}_i}(\Phi,\phi_1)*\sin\Phi\cdot\cos k\Phi\cdot\sin(m\phi_1)\, d\Phi\, d\phi_1 \tag{12b}$$

and later passing from an orthogonal basis to another:

$$P_l^{m0}(\Phi) = \sum_{s=-l}^{+l} a^{m0s}\cdot e^{is\Phi} \tag{13}$$

where

$$a_l^{m0k} = \frac{(-1)^{\nu+m}}{2^{2l}} *(l-k)!(l+k)!(l+m)!(l)!\sqrt{\frac{(l-m)!}{(l+m)!}} * \\ *\sum_{\nu=0}^{l-k}\frac{(-1)^k}{(l-m-\nu)!(m+k+\nu)!(l-k-\nu)!\nu!}* \\ *\sum_{\nu=0}^{l}\frac{(-1)^\nu}{(l-k-\nu)!(k+\nu)!(l-\nu)!\nu!} \tag{14}$$

and therefore [11,12].

$$F_l^m(\vec{h}_i) = \sum_{k=0(2)}^{\infty} \sum_{m=-l(2)}^{+l} a_l^{m0k} \int_0^{\frac{\pi}{2}} \int_0^{2\pi} P_{\vec{h}_i}(\Phi,\phi_1) * \cdot \quad (15)$$

$$* \sin\Phi \cdot \cos k\Phi \cdot e^{im\phi_1} d\Phi d\phi_1$$

TABLE 1

The comparison of the calculated values of the elastic and shear moduli with those measured by Rosinger et al [4].

a). Elastic modulus, E[GPa]

Texture	Orientation	Measured	Calculated
Cold worked	axial	94,62	95,95
	tangential	94,60	96,56
Recrystal-lized	axial	96,64	95,76
	tangential	96,92	96,47
Isotropic	-	95,0	95,31

b). Shear modulus G[GPa]

Texture	Orientation	Measured	Calculated
Cold worked	axial	34,04	39,33
	tangential	34,14	39,38
Recrystal-lized	axial	35,09	39,34
	tangential	35,25	39,32
Isotropic	-	33,82	39,2

The modelling of the G^{-1} elastic modulus was performed on a IBM-PC computer for the three textures analyzed for the temperatures: 573 K, 723 K (just before primary recrystallization, the case of an acceptable temperature excursion) and for 1173 K (the case of a Loss of Coolant Accident, with large temperature excursions, when the texture changes

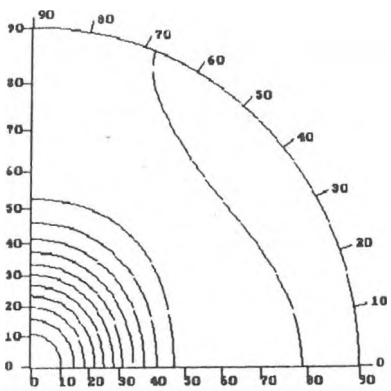

(a)

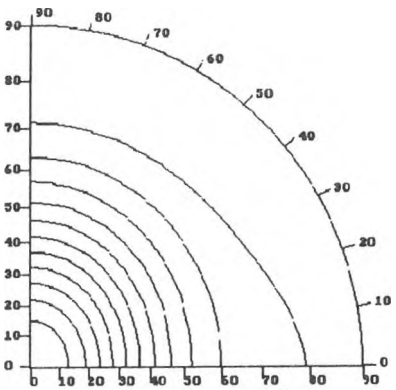

(b)

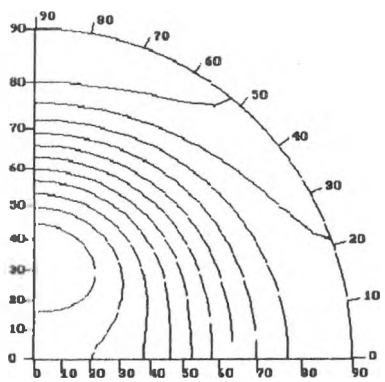

(c)

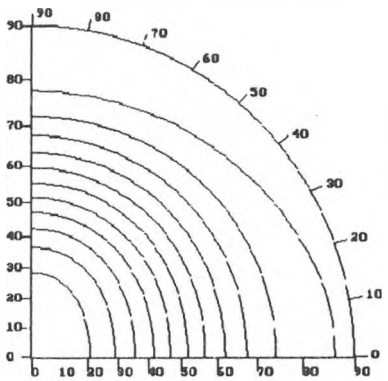

(d)

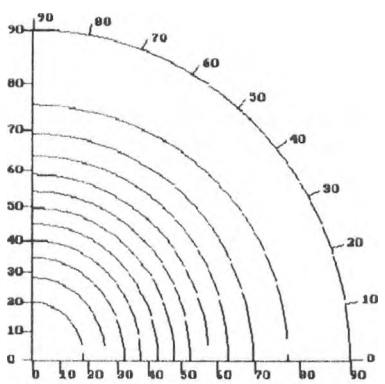

(e)

Fig. 3. The result of the modelling for the inverse shear modulus, G^{-1}:
(a)-cold worked texture, 573 K;
(b)-recrystallized texture, 723 K;
(c)-β transformed texture, 573 K;
(d)-β transformed texture,723 K;
(e)-β transformed texture,1173 K;

twice, from the cold worked type to the recrystallized and then to the beta transformed type); in the later case only the β transformed texture was considered since any primary metallurgical state will transform to this one. The results yielded are presented in Fig. 3. Table 1 summarizes a comparison of our results with the measurements performed by others.

5. CONCLUSIONS. The measured and calculated values fairly agree within the 5% error usually considered [3-7]. One may observe that the main modifications in the elastic anisotropy do not appear in the principal directions but at the polar angle 45°, in the tangential direction for the cold worked and recrystallized textures and in the axial direction for the β transformed texture respectively. It is important to note that this anisotropy may not be conveniently measured given the shape of the fuel sheathing. However, the calculation we have presented allows a proper evaluation of any of the elastic moduli.

REFERENCES

[1]. I. Ursu, "Fizica şi tehnologia materialelor nucleare", Ed. Academiei, Bucureşti, 1982.
[2]. R.J. Roe, J.Appl.Phys, 36(1965)2024.
[3]. H.J. Bunge, "Mathematische Methoden der Textur Analyse", Akademie Verlag, Berlin, (1969).
[4]. H.S. Rosenbaum und J.E.Lewis, J.Nucl.Mater., 67(1977)273.
[5] N. Nakatsuka, Nucl. Eng. and Des., 65(1981)103.
[6]. W.R. Catlin, D.C. Lord, F. Zaverl and D. Lee, J. of Nucl. Mater., 68(1977)345.
[7]. D.O. Northwood, I.M. London and L.E. Bahen, J. of Nucl.Mater., 55(1975)299.
[8]. H.E. Rosinger and D.O. Northwood, J.of Nucl.Mater., 79(1979)170.
[9]. E.S. Fisher and C.J. Renken, J.of Nucl.Mater., 4(1961) 311.
[10]. E.S. Fisher and C.J. Renken, Phys.Rev. A, 135(1964)482.
[11]. D. Ciurchea, J. of Nucl. Mater., 101(1985)1.
[12]. D. Ciurchea, Ph.D. Thesis, Cluj-Napoca, 1992.

STUDIA UNIV. BABEŞ-BOLYAI, PHYSICA, XXXIX, 2, 1994

ALGEBRAIC CHARACTERIZATION OF THE WESS-ZUMINO CONSISTENCY CONDITIONS IN BRST THEORY AND THE CONNECTION WITH THE PROBLEM OF CONSISTENT INTERACTION BETWEEN GAUGE FIELDS

G. BARNICH*, R. TĂTAR and L. TĂTAR*****

ABSTRACT. - The operator δ, introduced by Sorella, is used to solve the Wess-Zumino consistency condition for the problem of the consistent interaction between gauge fields.

1. INTRODUCTION. The Batalin-Vilkovisky (BV) method [1,2] for quantizing arbitrary gauge theories seems to be the most powerful and elegant one. The physical foundation of this method has been clarified by proving that gauge invariance is completely captured by the BRST symmetry and cohomology [3,4].

The algebraic structure of BV method has been developed in [5,6,7] where Batalin and Vilkovisky algebras are defined and are connected with topological field theory in two dimensions.

In a very interesting paper Marc Henneaux and one of us [8] have used the BV formalism to analyse the constructing consistent interactions among fields with gauge freedom. They proposed, in the antifield formalism, a scheme to find out the interaction lagrangian by using the deformation theory. In fact they deformed consistently the Master Equation and showed that there is no obstruction to constructing a perturbative solution to the Master Equation, unless one insists on locality. Even in this case it is possible to reformulate the deformation

* *Université Libre de Bruxelles, Faculté des Sciences, Campus Plaine C.P.231, B-1050 Bruxelles, Belgium*

** *University of Craiova, faculty of Science, 1100 Craiova, Romania*

*** *"Babeş-Bolyai" University, Faculty of Physics, 3400 Cluj-Napoca, Romania*

of the Master Equation that takes into account locality.

The basic equations in this new setting are the descent equations for an extended BRST cohomology which includes the fields as well the antifields. In this way they showed that the only Lorentz consistent covariant interactions for free (abelian) Chern-Simons models in 3-dimensions is given by non-abelian Chern-Simons theory.

In this letter we intend to apply the deformation theory for constructing a local, Lorentz covariant, consistent interaction for the abelian Chern-Siomons model in higher dimension.

The main question in our approach is to solve the descent equations, i. e., to find the elements of the cohomology group $H^0(s^{(0)},d)$ [9]. We shall use a new way of finding out non-trivial solution of the descent equations proposed by Sorella [9] and succesfully applied to the study of Chern-Simons cohomology, when one considers only the fields and not the antifields.

The method relies on the introduction of the operator of the operator δ which allows us to decompose the exterior derivative as a BRST commutator

$$d=[\delta,s] \tag{1}$$

where d is the exterior derivative, s is the BRST operator and δ is one operator introduced by Sorella, which does not have the property of being a derivative.

It is very easy to show that a solution of the descent equations is given by repeated applications of δ on a BRST-invariant polynomial of fields.

In the case of BV-method one has to modify the form of BRST transformation by introducing the antifields. Moreover, the method proposed by Sorella works also in this extended case and we shall apply it to find the deformation theory of the abelian Chern-

Simons in 5-dimensions and for Yang-Mills in four dimensions.

2. THE DEFORMATION PROBLEM FOR THE MASTER EQUATION. We will use in this section the notations of [8]. In fact, this will be a short review of that paper.

Let $S_0^{(0)}$ be a free action which may have the "free" gauge symmetries

$$\Phi^i \to \Phi^i + R^{(0)i}{}_\alpha \varepsilon^\alpha \ . \tag{2}$$

As it is well known in the BV method, a quantum action corresponding to the free action is a solution of the master equation for the free theory

$$(S^{(0)}, S^{(0)}) = 0 \tag{3}$$

with the proper boundary conditions.

Now the problem of constructing consistent interactions can be reformulated in terms of the master equation.

In [8] it has been shown that the problem of constructing consistent interactions for a free gauge theory can be naturally reformulated as a deformation problem of the master equation. If an interaction theory can be constructed, its consistency is expressed through the existence of the solution:

$$\begin{aligned} &S = S^{(0)} + gS^{(1)} + g^2 S^{(2)} + \ldots \\ &(S, S) = 0 \ . \end{aligned} \tag{4}$$

This consistency condition can be analysed order by order in the deformation parameter:

$$\begin{aligned} (S^{(0)}, S^{(0)}) &= 0 \\ 2(S^{(0)}, S^{(1)}) &= 0 \\ 2(S^{(0)}, S^{(2)}) + (S^{(1)}, S^{(1)}) &= 0 \end{aligned} \tag{5}$$

These equations are valid by cohomological reasons as argued in [9].

In [8] it was showed that if one starts from the abelian 3-dimensional Chern-Simons theory

and we consider the deformation of the master equation, we will arrive to non-abelian Chern - Simons theory.

Our first goal here is to show that the same result can be obtained if we introduce the Sorella's δ-operator.

3. THE δ AND G OPERATORS. In [9] Sorella has worked only with fields in the language of forms and he considered the nonabelian case.

If we consider now the abelian case for which the structure constants are 0 we will obtain the following form for the BRST and exterior derivative operators:

$$\begin{aligned} s &= \xi^a \frac{\partial}{\partial A^a} \\ d &= \xi^a \frac{\partial}{\partial c^a} + dA^a \frac{\partial}{\partial A^a} \end{aligned} \tag{6}$$

Starting from this , Sorella introduced the following operator in the abelian case

$$\delta = -A^a \frac{\partial}{\partial c^a} + dA^a \frac{\partial}{\partial dc^a} \tag{7}$$

This new operator has the important property that gives the decomposition of the exterior derivative as a BRST operator like (1).

We are interested to obtain the action of this operator on the antifields.

We will consider, in what follows a 3D Chern-Simons theory. For this the form of the BRST operator is given by:

$$s^{(0)} = \varepsilon^{ijk} F_{jka} \frac{\partial}{\partial A^{i*}_a} - \partial_i A^{i*}_a \frac{\partial}{\partial C^a} + \partial_i C^a \frac{\partial}{\partial A^a_i} \tag{8}$$

If we consider now the equation (1) with $s^{(0)}$ instead of s we will obtain the following action of Sorella's operator on the fields and antifields

$$\delta A=0,\delta C=-A,\delta A^*=C^*,\delta C^*=0 \tag{9}$$

The last of this equations is obtained from the condition that the minimum ghost is -2 and δ lowers the ghost by one unity.

We did not finish because we have to verify the other relation of Sorella. He also introduced the operator G which in the abelian case has the form $G=dA^a\frac{\partial}{\partial c^a}$ and satisfies the following relation

$$[d,\delta]=2G\ . \tag{10}$$

Starting from the relation, we will obtain that the action of this operator on the fields and antifields will be given by

$$GA=0,\ GC=-dA,\ GA^*=0,\ Gc^*=0\ .$$

We have to make one remark. While G is a nilpotent operator, δ has not this property because it is an operator of even dimension.

We introduce the generalization of these operators when the antifields are taken into account.

For Chern-Simons theory in n dimensions, Sorella showed that the solution to the descent equations

$$\begin{aligned}\omega_0^{2n+1}&=Tr(\frac{c^{2n+1}}{(2n+1)!})\\ \omega_{2p}^{2n+1-2p}&=\frac{\delta^{2p}}{(2p)!}\omega_0^{2n+1}-\sum_{j=0}^{p-1}\frac{\delta^{2j}}{(2j)!}\Omega_{2p-2j}^{2n+1-2p+2j}\end{aligned} \tag{13}$$

for the even space-time form sector and with one more δ for the odd sector.

One example of applying this formulas appears for the 3D Chern-Simons theory.

In this case, if we start from the descent equations

$$\begin{aligned} s^{(0)}a_{[3]}+da_{[2]}&=0\\ s^{(0)}a_{[2]}+da_{[1]}&=0\\ s^{(0)}a_{[1]}+da_{[0]}&=0\\ s^{(0)}a_{[0]}&=0 \end{aligned} \tag{14}$$

where $a_{[3]}=L_1$ which appears in [8] and the solution for the bottom is taken to be $a_{[0]}=f_{abc}c^{a}c^{b}c^{c}$ (the reasons can be found in [8,10]) we will obtain the following expressions for $a_{[3]}$

$$a_{[3]}=\frac{1}{3!}\delta^{3}a_{[0]}-\delta\Omega_{2}^{1} \tag{15}$$

where Ω_2^{1} is given by $s^{(0)}\Omega_2^{1} = Ga_{[0]}$

If we perform the calculus we will obtain that

$$a_{[3]} = -f_{abc}A_i^{a}A_j^{b}A_k^{c}\varepsilon^{ijk}-\frac{3}{2}f_{bc}^{a}\tilde{C}^{*}_{a}C^{b}C^{c}+3f_{bc}^{a}\tilde{A}^{*}_{ia}A^{ib}C^{c} \tag{16}$$

which is , up to a constant, the same result with that obtained in [8], so the solution of the descent equations is given by the interaction density. The tilded variables are dual of the untilded ones

So we have obtained by Sorella's method the same thing as in [8].

Now we will apply the same method to the Yang-Mills case. As was shown in [11] the only possibility to solve the descent equations is to leave from $a_{[2]}$ which must be taken under the form

$$a_{[2]} = f_{abc}\tilde{F}C^{b}C^{c} \tag{17}$$

For the Yang-Mills field we have the same equations, the only difference will be that we will need also

$$\delta \tilde{F} = -\tilde{A}^{*} \tag{18}$$

In this case we will obtain

$$a_{[4]}=\frac{1}{2}\delta^{2}a_{[2]}-\Omega_{2}^{1} \tag{19}$$

where Ω_2^1 is given by

$$s^{(0)}\Omega_{2}^{1}=-2f_{ABC}\tilde{F}^{a}\tilde{F}^{b}C^{c} \tag{20}$$

If the structure constants are totally antisymmetric, the right-hand side of the previous equation will give 0 and that means that $\Omega_2^1=0$.

So $a_{[4]}$ will given by L_1 of [11] up to some constants.

We showed that for Chern-Simons in 3D and for Yang-Mills in 4D we obtain the same result as in [8] and [11] when apply the Sorella's formalism.

The things become more difficult if we go to Chern-Simons in higher dimensions.

For five dimensions we start from the following action

$$S_{0}^{(0)}=\int d^{5}x\ \varepsilon^{ijklmn}A_{i}F_{jk}F_{mn} \tag{21}$$

If we start from the bottom of the consistency conditions, we will obtain the Sorella's formula for 5D Chern-Simons theory

$$a_{[5]}=\frac{1}{5!}\delta^{5}a_{[0]}-\frac{1}{3!}\delta^{3}\Omega_{2}^{3}-\delta\Omega_{4}^{1} \tag{22}$$

If we take as the bottom the term $a_{[0]} = d_{ab}f_{bmn}f_{cpq}c^{a}c^{m}c^{n}c^{p}c^{q}$, the first term in the equation (14) will be something proportional with A^5 because δ will anihilate the fields A.

It remains to obtain Ω_2^3, Ω_4^1. If we apply G on $a_{[0]}$ we will obtain a term which is

proportional with F. Unfortuately, it is impossible to obtain such a term as a result of the action of $s^{(0)}$. The only way to surpass the difficulty is to consider the action of $s^{(0)}$ on $\tilde{A}^{i*}$ which will give an action which is proportional with F^2. In fact

$$s^{(0)}\tilde{A}^{i*}=\varepsilon^{ijklm}F_{jk}F_{lm} \tag{23}$$

So the way we were working for the action in dimensions lower than 5 cannot, in principle, apply here because we do not obtain the terms Ω which would have to enter in the expression of the $a_{[n]}$ where n is the dimension of the space in which we are working. In the case of 3D Chern-Simons theory and Yang-Mills theory, the BRST transformation of $\tilde{A}^{i*}$ was proportional with F, exact the term which appeared after the action of G on c.

We can start also from the other level, with $a_{[3]} = d^{abc}\tilde{F}^{a}c^{b}c^{c}$ and to give the following formula

$$a_{[5]} = \delta^2 a_{[3]} - \Omega_2 \tag{24}$$

In this case would have the difficulty of calculating $\delta\tilde{F}^{a}$ because this case is more complicated than the Yang-Mills case.

Thus as a conclusion, Sorrela's approach seems to give some difficulties for higher dimensions.

REFERENCES

[1]. I.A. Batalin and G. A. Vilkovisky, Phys. Lett. 102B(1981) 27; Phys. Rev. D28(1983)2567.

[2]. M. Henneaux and C. Teitelboim, Quantization of Guage Systems, Princeton University Press, Princeton 1992.

[3]. J. Fisch, M. Henneaux, J. Stasheff and C. Teitelboim, Comm. in Math. Phys. 120 (1989)379.

[4]. J. Fisch and M. Henneaux, Comm. in Math. Phys. 128(1990)627.

[5]. M.Penkava and A. Scharz, "On some algebraic structure arising in the string theory", preprint

hepth/9212072.

[6]. E. Getzler, "Batalin-Vilkovisky algebra and two dimensional topological field theories", preprint hepth/9212043 .

[7]. E. Getzler and J. D. S. Jones, "n-Algebras and Batalin-Vilkovisky algebras", MIT-preprint (1993).

[8]. G. Barnich and M. Henneaux, "Consistent couplings between fields with a gauge freedom and deformations of the master equation", ULB-PMIF-93/01(1993).

[9]. S. P. Sorella, "Algebraic characterization of the Wess-Zumino consistency conditions in gauge theories", UGVA-Dpt 1992/08-781.

[10]. F. Brandt, N. Dragon, M. Kreutzer, Nucl. Phys. B332(1990)224 M. Dubois-Violette, M. Henneaux, M. Talon, C.M. Viallet, Phys. Lett. B(1992)23.

[11]. G. Barnich, M. Henneaux, R. Tatar, Int. Journ. of Mod. Phys. D(1994)139-144.

STUDIA UNIV. BABEŞ-BOLYAI, PHYSICA, XXXIX, 2, 1994

SOME EXACT SOLUTIONS OF CHARGED FLUID SPHERES IN GENERAL RELATIVITY

S. BALLAI* **and Al. MARCU***

ABSTRACT. - The paper present a family of interior solution of the Einstein - Maxwell field equations in general relativity for a static, spherically symmetric distribution of charged fluid. The family of solution have been matched with the Reissner-Nordstrom metric at the boundary.

1. INTRODUCTION

The Einstein - Maxwell field equation in the presence of matter and charge form a highly non - linear system of equations. So a small number of exact solutions have been obtained . Bonnor (1960) , Efinger (1965) , Kyle and Martin (1967) , Krory and Barna (1975) , Nduka (1976 , 1977) , Singh and Yadav (1978) have been obtained internal solutions for static spherically symmetric charged fluid spheres under different conditions .

For the charged static spherically symmetric fluid of density ρ , pressure p and total charge Q , the field equations reduce to three complete ordinary differential equations , involving the fluid variables and two metric functions . In order to solve this system , it is necessary to specify in some manner two of unknown or to introduce subsidiary relation between them i. e. specily on equations of state .

In the present paper we have obtained some exact solutions for the spherical symmetric charged fluid distribution using an entirely different technique , namely a specific choice of metric function $\nu(r)$ and charge $Q(r)$

* *"Babeş-Bolyai" University, Faculty of Physics, 3400 Cluj-Napoca, Romania*

2. THE FIELD EQUATIONS AND THEIR SOLUTIONS

We use here the spherically symmetric line element

$$ds^2=e^{\nu}\cdot c^2\cdot dt^2-e^{\lambda}\cdot dr^2-r^2\cdot(d\theta^2+\sin^2\theta\cdot d\varphi^2) \qquad (2.1)$$

where λ and ν are function of r only.

In general relativity , the Einstein-Maxwell equations for the charged fluid are :

$$G_{ij}=\frac{8\pi\cdot G}{c^4}\cdot T_i^k \qquad (2.2)$$

$$[(-g)^{\frac{1}{2}}\cdot F^{ij}]_{,j}=4\pi J^i\cdot(-g)^{\frac{1}{2}} \qquad (2.3)$$

$$F^{ij}{}_{,k}=0 \qquad (2.4)$$

where i,j,k=0,1,2,3

T_i^k is the energy momentum tensor, J^i is the current four vector and

$$G_{ij}=R_i^k-\frac{1}{2}\cdot g_i^k\cdot R$$

is the Einstein tensor with R_{ij} as the Ricci tensor and R the scalar of curvature tensor .

For the system under study the energy momentum tensor T_i^j has two parts viz . t_j^i and E_j^i for matter and charges respectively

$$T_j^i=t_j^i+E_j^i \qquad (2.5)$$

where

$$t_j^i=\rho\cdot u^i\cdot u_j+p\cdot\delta_j^i-\sigma_j^i \qquad (2.6)$$

where σ_j^i is the viscosity strain tensor

$$\sigma_j^{\ i}=\eta\cdot\left(\frac{\partial u^{\ i}}{\partial x_k}+\frac{\partial u^{\ k}}{\partial x_i}-\frac{2}{3}\cdot\delta_k^{\ i}\cdot\frac{\partial u^{\ l}}{\partial x_l}\right)+\xi\cdot\delta_k^{\ i}\cdot\frac{\partial u^{\ l}}{\partial x_l} \qquad (2.7)$$

with $u^i u_i = 1$ and

η - cinematic viscosity coefficient

ξ - dynamic viscosity coefficient

The nonvanishing components of t_j^i are

$$t_1^{\ 1}=p-2\cdot\eta\cdot\frac{\partial u^{\ 1}}{\partial x_1}+\left(\frac{2}{3}\cdot\eta-\xi\right)\cdot\frac{\partial u^{\ l}}{\partial x_l} \qquad (2.8)$$

$$t_2^{\ 2}=p-2\cdot\eta\cdot\frac{\partial u^{\ 2}}{\partial x_2}+\left(\frac{2}{3}\cdot\eta-\xi\right)\frac{\partial u^{\ l}}{\partial x_l} \qquad (2.9)$$

$$t_3^{\ 3}=p-2\cdot\eta\frac{\partial u^{\ 3}}{\partial x_3}+\left(\frac{2}{3}\cdot\eta-\xi\right)\cdot\frac{\partial u^{\ l}}{\partial x_l} \qquad (2.10)$$

$$t_0^{\ 0}=\rho+p-2\cdot\eta\cdot\frac{\partial u^{\ 0}}{\partial x_0}+\left(\frac{2}{3}\cdot\eta-\xi\right)\cdot\frac{\partial u^{\ l}}{\partial x_l} \qquad (2.11)$$

where u^i is the velocity fourth vector

The electromagnetic energy tensor E_j^i in terms of field tensor F_{ij} is given by :

$$4\cdot\pi\cdot E_k^{\ i}=-F^{\ il}\cdot F_{kl}+\frac{1}{4}\cdot\delta_k^{\ i}\cdot F^{\ hl}\cdot F_{ne}+\gamma\cdot\left(A^{\ i}\cdot A_k-\frac{1}{2}\cdot\delta_k^{\ i}\cdot A_l\cdot A^{\ l}\right) \qquad (2.12)$$

Where A^i is the components of the potential vector

Due to spherical symmetry , the only non - vanishing components of field tensor F^{ij}

are $F^{01} = - F^{10}$

Then the nonzero components of E_j^i are :

$$E_0^{\,0}=E_1^{\,1}=-E_2^{\,2}=-E_3^{\,3}=-\frac{1}{8\pi}\cdot g_{00}\cdot g_{11}\cdot(F^{01})^2 \qquad (2.13)$$

By this choice of field tensor F^{ij} equation (2.4) is clearly satisfied .

From equation (2.3) we get :

$$F^{01}=\frac{Q(r)\cdot e^{-\theta}}{r^2} \qquad (2.14)$$

Where $\theta = (\lambda + \nu)/2$ and Q(r) represents the total charge within a sphere of radius r , viz.

$$Q(r)=4\pi\cdot\int_0^r J^0\cdot r^2\cdot e^{\theta}\cdot dr \qquad (2.15)$$

From equation (2.3) we can see that outside the fluid sphere Q(r) is a constant Q_0 (the total charge) . Then from (2.14) one finds the asymptotic form of the electric field Q_0/r^2 .

Thus the field equation may be written :

$$\frac{8\pi G}{c^4}[p-2\eta\frac{\partial u^1}{\partial x_1}+(\frac{2}{3}t\eta-\xi)\frac{\partial u^l}{\partial x_l}]+\frac{8\pi G}{c^4}E_1^{\,1}=-e^{-\lambda}(\frac{\nu'}{r}+\frac{1}{r^2})+\frac{1}{r^2} \qquad (2.16)$$

$$\frac{8\pi G}{c^4}[p-2\eta\frac{\partial u^2}{\partial x_2}+(\frac{2}{3}\eta-\xi)\frac{\partial u^l}{\partial x_l}]+\frac{8\pi G}{C^4}E_2^{\,2}=-e^{-\lambda}(\frac{\nu''}{2}+\frac{\nu'^2}{4}+\frac{\nu'-\lambda'}{2r}-\frac{\lambda'\nu'}{4}) \qquad (2.17)$$

$$\frac{8\pi G}{c^4}[\rho+p-2\eta\frac{\partial u^0}{\partial x_0}+(\frac{2}{3}\eta-\xi)\frac{\partial u^l}{\partial x_l}]+\frac{8\pi G}{c^4}E_0^{\,0}=e^{-\lambda}(\frac{\lambda'}{r}-\frac{1}{r^2})+\frac{1}{r^2} \qquad (2.18)$$

Eliminating p from (2.16) and (2.17) noting that :

$$y=e^{\frac{\nu}{2}} \quad \Rightarrow \quad \nu=2\cdot\ln y \qquad (2.20)$$

Using equation (2.14) , (2.19) the second order differential equation :

$$y'' - (\frac{1}{r} + \frac{\lambda'}{2})y' + [\frac{e^{\lambda}}{r^2} - \frac{\lambda'}{2r} - \frac{1}{r^2} - e^{\lambda}[2\eta(\frac{\partial u^2}{\partial x_2} - \frac{\partial u^1}{\partial x_1}) - \frac{1}{4\pi}\frac{Q^2(r)}{r^4}]\frac{8\pi G}{c^4}]y = 0 \quad (2.20)$$

is the generalization of Wyman's equation (Wyman 1949) let us assume that total charge Q is given by :

$$Q(r) = k\, r \quad (2.21)$$

Where k is a proportionality constant .

We consider :

$$\frac{\partial u^2}{\partial x_2} - \frac{\partial u^1}{\partial x_1} = \Lambda \quad (2.22)$$

where Λ is constant and :

$$\frac{8 \cdot \pi \cdot G}{c^4} = \beta = 2{,}06 \cdot 10^{-43} \quad (2.23)$$

From (2.20) - (2.23) we obtain :

$$y'' - (\frac{1}{r} + \frac{\lambda'}{2}) \cdot y' + [\frac{e^{\lambda}}{r^2} - \frac{\lambda'}{2r} - \frac{1}{r^2} - e^{\lambda}(2 \cdot \eta \cdot \Lambda - \frac{1}{4 \cdot \pi} \cdot \frac{k^2}{r^2}) \cdot \beta] \cdot y = 0 \quad (2.24)$$

Now we define :

$$e^{-\lambda} = \tau(r) \quad (2.25)$$

Then equation (2.24) in therms of $\tau(r)$ becomes :

$$\tau'(r)-\tau(r)\cdot\left[\frac{2\cdot(y+r\cdot y'-r^2\cdot y'')}{r\cdot(y+r\cdot y')}\right]=\frac{-2\cdot y\cdot\left(1+\frac{1}{4\pi}\cdot k^2\cdot\beta-2\cdot\eta\cdot\Lambda\cdot r^2\cdot\beta\right)}{r\cdot(y+r\cdot y')} \qquad (2.26)$$

The (2.26) solution is :

$$\tau(r)=\exp[-F(r)]\cdot\left\{\int_0^r \exp[F(r)]\cdot g(r)\cdot dr+C\right\} \qquad (2.27)$$

Where :

$$f(r)=\frac{-2\cdot(y+r\cdot y'-r^2\cdot y'')}{r\cdot(y+r\cdot y')} \qquad (2.28)$$

$$g(r)=\frac{-2\cdot y\cdot\left(1+\frac{1}{4\pi}\cdot k^2\cdot\beta-2\cdot\eta\cdot\Lambda\cdot\beta\cdot r^2\right)}{r\cdot(y+2\cdot y')}=\frac{-2\cdot y\cdot(\alpha-\gamma\cdot r^2)}{r\cdot(y+r\cdot y')} \qquad (2.29)$$

$$F(r)=\int_0^r f(r)\cdot dr \qquad (2.30)$$

and :

$$\alpha=1+\frac{1}{4\pi}\cdot k^2\cdot\beta$$

$$\gamma=2\cdot\eta\cdot\Lambda\cdot\beta$$

C is integration constant this value will be fixed by boundary conditions .

3. Model solution

Our purpose is to find the solution of equation (2.24) . Wilson (1969) , Nduka (1976) , Krori and Barua (1975) have solved this by imposing various conditions that simplify the equation and allow immediate integration . Once ν and λ are obtained , ρ and p follow directly from equation (2.17) , (2.18) . Equation (2.27) together with (2.14),

(2.17) , (2.18) and (2.21) represents all solutions for the static spherically symmetric charged fluid bodies .

- As a matter of fact ; one should not hope that all solution will be physically reasonable . Only a subclass of these solutions corresponding to certain functions $\nu(r)$ will be physically reasonable . Hence a specific choice of $\nu(r)$ is essential . Here we specify $\nu(r)$ in such a manner that equation (2.20) can be immediately integrated . Such a choice is that y satisfies the equation :

$$r^2 \cdot y'' - r \cdot y' - (1 - \alpha + \gamma r^2) \cdot y = 0 \qquad (3.1)$$

for p = -1

$$q = -(1 - \alpha + \gamma \cdot r^2)$$

(3.1) is transformed into well know Euler's equation :

$$r^2 \cdot y'' + p \cdot r \cdot y' + q \cdot y = 0 \qquad (3.2)$$

The indical equation far (3.2) is :

$$m^2 + (p-1) \cdot m + q = 0 \qquad (3.3)$$

Three different cases arise depending on the value of discriminant (Ritger and Rase 1968)

$$\Delta = (p-1)^2 - 4 \cdot q \qquad (3.4)$$

Case 1. $\Delta > 0$. This requires :

$$k^2 < \frac{4 \cdot \pi}{\beta} + 8 \cdot \pi \cdot \eta_1 \cdot \Delta \cdot r^2$$

The solution is :

$$y = a_1 \cdot r^l + b_1 \cdot r^m \qquad (3.5)$$

where a_1 and b_1 are constants to be fixed by boundary conditions and : $l = 1 + \mu$, $m = 1 - \mu$ for :

$$\mu=\sqrt{1-\frac{1}{4\pi}\cdot k^2\cdot\beta+2\eta\cdot\Lambda\cdot r^2}=\sqrt{\alpha'+\gamma\cdot r^2} \qquad (3.6)$$

with :

$$\alpha'=1-\frac{1}{4\pi}\cdot k^2\cdot\beta$$

Now we can calculate the $\tau(r)$ but his form is too complicate so we utilize the general expression . Hence from equation (2.16) and (2.18) density ρ and pressure p are given by :

$$p=2\eta\Lambda_1-(\frac{2}{3}\eta-\xi)\frac{\partial u^1}{\partial x_1}+\frac{1}{8\pi}\cdot\frac{k^2}{r^2}+\frac{1}{r^2}-\frac{3\tau_1(r)}{r^2}-\frac{2\tau_1(r)}{r^2}\frac{a_1r^{2\mu}-b_1}{a_1r^{2\mu}+b_1}(\mu+\frac{\gamma r^2\ln r}{\mu}) \qquad (3.7)$$

and :

$$\rho=\frac{2\tau_1(r)}{r^2}\cdot[1+\frac{a_1r^{2\mu}-b_1}{a_1r^{2\mu}+b_1}\cdot(\mu+\frac{\gamma\cdot r^2\ln r}{\mu})]-\frac{\tau_1(r)}{r}-2\eta\cdot(\Lambda_1-\Lambda_0) \qquad (3.8)$$

where :

$$\Lambda_1=\frac{\partial u^1}{\partial x_1}=ct$$

$$\Lambda_0=\frac{\partial u^0}{\partial x_0}=ct$$

We now impose the following boundary conditions :

1. The function $e^{-\lambda}$ i.e. $\tau(r)$ is continuous across the boundary *($r = r_0$)* of the fluid sphere.
2. The function e^{ν} and $\nu' e^{\nu}$ is continuous across the boundary *($r = r_0$)* of the fluid sphere.

The line element for $r > r_0$ is given by the Reissner - Nordstrom metric

$$ds^2=(1-\frac{2GM_0}{r}+\frac{GQ_0^2}{r^2c^4})c^2dt^2-\frac{dr^2}{(1-\frac{2GM_0}{r}+\frac{GQ_{0_2}}{r^2c^4})}-r^2(d\theta^2+\sin^2\theta d\varphi^2) \qquad (3.9)$$

where $Q_0 = Q(r_0)$ and M_0 is the total mass of the sphere given by :

$$M=4\pi\cdot\int_0^{r_0}\rho(r)\cdot r^2\cdot dr \qquad (3.10)$$

Using the above boundary condition the two constants of integration a_1 and b_1 are given by :

$$a_1=\frac{\sqrt{N}}{2\cdot r_0^{1+\mu}}\cdot\left[1+\frac{\mu\left(N+\frac{G\cdot Q_0^2}{c^4\cdot r_0^2}+1\right)}{2\cdot(\mu^2+\gamma\cdot r_0^2\cdot lnr_0)}\right] \qquad (3.11)$$

$$b_1=\frac{\sqrt{N}}{2\cdot r_0^{1-\mu}}\cdot\left[1+\frac{\mu\left(N+\frac{G\cdot Q_0^2}{c^4\cdot r_0^2}+1\right)}{2\cdot(\mu^2+\gamma\cdot r_0^2\cdot lnr_0)}\right] \qquad (3.12)$$

where :

$$N=1-\frac{2\cdot M_0\cdot G}{r_0}+\frac{G\cdot Q_0^2}{c^4\cdot r_0^2}$$

Case 2. $\Delta = 0$ i. e.

$$k^2=\frac{4\cdot\pi}{\beta}+8\cdot\pi\cdot\eta\cdot\Lambda\cdot r^2$$

The solution in these case is :

$$y=r(a_2\cdot lnr+b_2) \qquad (3.13)$$

and

$$\tau(r)=e^{-\lambda}=1+C_2\cdot e^{\frac{2\cdot b_2}{a_2}}\cdot(2\cdot a_2\cdot\ln r+2\cdot b_2+a_2)^{-1}\cdot r^2 \qquad (3.14)$$

where a_2, b_2, c_2 are constants to be fixed by boundary conditions :

$$a_2=\frac{1}{2\cdot r_0\sqrt{N}}\cdot(1-3\cdot N-\frac{G\cdot Q_0^2}{c^4\cdot r_0^2}) \qquad (3.15)$$

$$b_2=\frac{\sqrt{N}}{r_0}-\frac{lnr_0}{2\cdot r_0\sqrt{N}}\cdot(1-3\cdot N-\frac{G\cdot Q_0^2}{c^4\cdot r_0^2}) \qquad (3.16)$$

$$c_2=(N-1)\exp(-\frac{2\cdot b_2}{a_2})\cdot(\frac{2\sqrt{N}}{r_0}+a_2)\cdot r_0^{-2} \qquad (3.17)$$

Now , the pressure p and density ρ is :

$$p=2\eta\Lambda_1-(\frac{2}{3}\eta-\xi)\frac{\partial u^{\epsilon}}{\partial x_{\epsilon}}+\frac{1}{8\pi}\cdot\frac{k^2}{r^2}+\frac{1}{r^2}-\frac{\tau_2(r)}{r^2}(\frac{2a_2lnr+2b_2+2a_2}{a_2lnr+b_2}+1) \qquad (3.18)$$

$$\rho=\frac{2\tau_2(r)}{r^2}\frac{a_2lnr+b_2+a_2}{a_2lnr+b_2}-4c_2e^{\frac{2b_2}{a_2}}\frac{a_2lnr+b_2}{2a_2lnr+2b_2+a_2^2}-2\eta(\Lambda_1-\Lambda_0) \qquad (3.19)$$

where N has the same meaning as in case 1 .

Case 3. $\Delta < 0$ i. e.

$$k^2>\frac{4\cdot\pi}{\beta}+\gamma\cdot\pi\cdot\xi\cdot\Lambda\cdot r^2$$

The root of the indical equation (3.3) are conjugate complex numbers :

$$m_1=\sigma+i\cdot\delta \qquad m_2=\sigma-i\cdot\delta$$

where :

$$\alpha = 1 \ ;$$
$$\delta = \sqrt{\alpha+\gamma r^2}$$

The solution in this case is :

$$y=r^{\sigma}\cdot(\psi_1\cdot r^{i\delta}+\psi_2\cdot r^{-i\delta}) \qquad (3.19)$$

where Ψ_1 and Ψ_2 are constants . These solution can be expressed in terms of real functions by noting that :

$$r^{i\delta}=e^{i\delta\cdot lnr}=\cos(\delta\cdot lnr)+i\cdot\sin(\delta\cdot lnr) \qquad (3.20)$$

Hence the solution (3.19) can be written as :

$$y=r^{\delta}\cdot[a_3\cdot\cos(\delta\cdot lnr)+b_3\cdot\sin(\delta\cdot lnr) \qquad (3.21)$$

Where a_3 and b_3 are constants to be fixed by boundary conditions :

$$a_3=\frac{\sqrt{N}}{r_0}\cos(\delta_0 lnr_0)+\frac{\sqrt{N}}{2r_0}\cdot\frac{\delta_0(N+\frac{GQ_0^2}{c^4r_0^2}+1)}{(\delta_0^2+\gamma r_0^2 lnr_0)}\sin(\delta_0 lnr_0) \qquad (3.22)$$

$$b_3=\frac{\sqrt{N}}{r_0}\sin(\delta_0 lnr_0)-\frac{\sqrt{N}}{2r_0}\cdot\frac{\delta_0(N+\frac{GQ_0^2}{c^4r_0^2}+1)}{(\delta_0^2+\gamma r_0^2 lnr_0)}\cos(\delta_0 lnr_0) \qquad (3.23)$$

$$\delta_0=\sqrt{\alpha+\gamma\cdot r_0^2}$$

Using the equations (2.16) , (2.18) , the pressure p and the density ρ are given by

$$p_3=2\eta\Lambda_1-(\frac{2}{3}\eta-\xi)\frac{\partial u^a}{\partial x_a}+\frac{1}{8\pi}\frac{k^2}{r^2}+\frac{1}{r^2}-\frac{\tau_3(r)}{r^2}-2\tau_3(r)\cdot$$
$$\cdot[\frac{1}{r^2}+(\frac{\gamma\cdot r\cdot lnr}{\delta}+\frac{\delta}{r})\frac{b_3-a_3\cdot tg(\delta\cdot lnr)}{a_3+b_3\cdot tg(\delta\cdot lnr)}] \qquad (3.24)$$

$$\rho_3=2\cdot\tau_3(r)\cdot[\frac{1}{r^2}+(\frac{\gamma\cdot r\cdot lnr}{\delta}+\frac{\delta}{r})\cdot\frac{b_3-a_3\cdot tg(\delta\cdot lnr)}{a_3+b_3\cdot tg(\delta\cdot lnr)}]-$$
$$-\frac{\tau'_3(r)}{r}-2\cdot\eta\cdot(\Lambda_1-\Lambda_0)$$

where N has the same meaning as in cases 1 and 2 .

In addition the conditions $p \geq 0$ and $\rho \geq 0$ in the interior of the fluid sphere will impose further conditions on these solutions. We therefore restrict our solutions to those values of the constants for witch the pressure and density are positive .

If we put G=c=1 and $\eta=\xi=\lambda_1=0$ we obtain the Singh-Yadav solutions .

REFERENCES

Adler, R.J. : J. Math. Phys. 15,727,(1974)
Adler, R.J. : Bazin M. , Schiffer , M. M. : Introduction to General Relativity , McGraw - Hill ,New - York 1974
Bonner, W. B., : Z. Phys. 160,59, (1960)
Efinger, H., J, : Z. Phys. 188,31, (1965)
Krori, K. D., Barna, J. ; J. Phys. A8,508, (1975)
Kyle, C. F., Martin, A. W. : Nuovo Cimento 50,583, (1967)
Landau L. D., Lifsic E. M. : Electrodinamica mediilor continue (l. magh.) Tankonyvkiado , Budapest 1986
Nduka, A. : General Relativity . Gravitation 7,501,(1976)
Nduka, A. : Acta Phys. Pol. B8,75, (1977)
Ritger, P. D., Rose N. Ǝ. : Differential Equations with Applications , McGraw - Hill , New - York 1968
Singh, T., Yaday, R. B. S. : Acta Phys. Pol. B6,475 (1978)
Wilson, S. J. : Can J Phys. 47,2401, (1969)
Wyman, M. : Phys. Rev. 75,1930, (1949)

În cel de al XXXIX-lea an (1994) *Studia Universitatis Babeş-Bolyai* apare în următoarele serii:
matematică (trimestrial)
fizică (semestrial)
chimie (semestrial)
geologie (semestrial)
biologie (semestrial)
filozofie (semestrial)
sociologie-politologie (semestrial)
psihologie-pedagogie (semestrial)
ştiinţe economice (semestrial)
ştiinţe juridice (semestrial)
istorie (semestrial)
filologie (trimestrial)
teologie ortodoxă (semestrial)
educaţie fizică (semestrial)

In the XXXIX-th year of its publication (1994) *Studia Universitatis Babeş-Bolyai* is issued in the following series:

mathematics (quarterly)
physics (semestrily)
chemistry (semestrily)
geology (semestrily)
geography (semesterily)
biology (semesterily)
philosophy (semesterily)
sociology-politology (semesterily)
psychology-pedagogy (semesterily)
economic sciences (semesterily)
juridical sciences (semesterily)
history (semesterily)
philology (quarterly)
orthodox theology (semesterily)
physical traning (semesterily)

Dans sa XXXIX-e année (1994) *Studia Universitatis Babeş-Bolyai* paraît dans les series suivantes:

mathematiques (trimestriellement)
physique (semestriellement)
chimie (semestriellement)
géologie (semestriellement)
géographie (semestriellement)
biologie (semestriellement)
philosophie (semestriellement)
sociologie-politologie (semestriellement)
psyhologie-pédagogie (semestriellement)
sciences économiques (semestriellement)
sciences juridiques (semestriellement)
histoire (semestriellement)
philologie (trimestriellement)
théologie ortodoxe (semestriellement)
éducation physique (semestriellement)